2017

Experimental Evaluation Of Compression Strength And Bleed Characteristics Of Cement-Based Grout Made With Photon Attenuating Inclusions

Abdulrahman Alfurayh
Lehigh University

EXPERIMENTAL EVALUATION OF COMPRESSION STRENGTH AND BLEED CHARACTERISTICS OF CEMENT-BASED GROUT MADE WITH PHOTON ATTENUATING INCLUSIONS

by

Abdulrahman Alfurayh

A Thesis

Presented to the Graduate Research Committee

of Lehigh University

in Candidacy for the Degree of

Master of Science

in

Structural Engineering

Department of Civil and Environmental Engineering

Lehigh University

Bethlehem, Pennsylvania

June 2017

This thesis is accepted and approved in partial fulfillment of the requirements for the Master of Science.

_____
Date

_____
Dr. Stephen Pessiki
Thesis Advisor

_____
Dr. Panayiotis Diplas
Chairperson of Department

ACKNOWLEDGEMENTS

First, I would like to thank my parents for their continual support, help, and love throughout my entire life.

Sincere thanks go to Dr. Stephen Pessiki, the research advisor. I am very grateful for his support, guidance, and help during my graduate study at Lehigh University.

I would like to thank the technicians who work in Fritz Laboratory and ATLSS for their assistant. Moreover, I would like to thank Michael Drury for his help with performing some experiments.

Finally, I'm very thankful for Qassim University for supporting me financially during my graduate study. Many thanks go to the Federal Highway Administration (FHWA) for their financial support for this research.

TABLE OF CONTENTS

LIST OF TABLES

LIST OF FIGURES

ABSTRACT

This research investigates the effect of adding high atomic number photon attenuating inclusions (PAI) within cementitious grout used in post-tensioned structures. Because of its advantageous attenuation characteristics, PAI can improve void detection in the target material by increasing contrast in radiographic images.

The research involved three experimental tests of grouts made with various ingredients of PAI materials; compression strength tests, bleed tests, and x-ray attenuation tests. In the grout compression tests, cementitious grout specimens were made with conventional grout as well as 10% and 20% weight fraction of PAI materials ($BaCO_3$ and Fe_2O_3) and 20% of Ottawa Sand, and tested at three different ages. In the bleed tests, tubular specimens were made for conventional grout and grout made with 20% weight fraction of $BaCO_3$, and their bleeding values were recorded up to two hours. In the radiography test, cylindrical specimens were made with concrete specimen as well as conventional grout and grouts made with 10% and 20% weight fraction of $BaCO_3$, and they were exposed to x-ray radiation for certain different times.

It was found that the tested PAI materials ($BaCO_3$ and Fe_2O_3) as well as Ottawa Sand do not have an adverse effect on the grout compression strength. From the bleed tests, it was found that adding barium carbonate within grout decreases significantly the amount of bleed water, comparing to conventional grout. Moreover, it was found that adding barium carbonate within grout increases its ability to attenuate the incident x-ray radiation.

CHAPTER 1

INTRODUCTION

1.1 INTRODUCTION

Post-tensioned (PT) structures have been constructed in the US since the early 1950s. Because of their ability to span farther with a lack of cracking and deflection, more PT structures are being and will be constructed.

In order to protect the prestressing strands from corrosion, and to provide adequate bond between the prestressing strands and surrounding structure, a cementitious-based grout is used. Of the main problems related to grout used in internal PT structures is how to detect internal defects, such as voids. Formation of voids within the grout can lead to major problems regarding the durability of strands. Accordingly, various nondestructive evaluation (NDE) techniques have been used for the inspection of post-tensioning structures.

The research in this report is related to radiographic inspection, where high energy x-ray or gamma ray radiation is used to produce a radiographic image of the internal structure of the test object. Keller & Pessiki (2016) showed that adding a high atomic number photon attenuating inclusion, specifically barium and iron, to the cementitious grout increases the attenuation of the grout. This increased attenuation may allow greater detectability of the grout, or more importantly, greater detectability of the absence of grout (i.e. voids).

Keller & Pessiki (2016) also tested grouts made with iron (high atomic number ingredient) and Ottawa Sand (a component commonly found in prepackaged grouts). Both

the barium carbonate and iron PAI materials increased the attenuation properties of the grouts. Keller & Pessiki (2016) only examined the attenuation properties of the grout. No work was performed to evaluate other properties such as strength and bleeding.

This report describes tests that were performed to evaluate the effect of adding PAI materials to the cementitious grout components on resulting grout properties, including compression strength, bleeding, and x-ray attenuation. Two of the three tests that were performed, compressive strength tests and bleed tests, are required by the Post-Tensioning Institute (PTI). In each test, at least two different grout materials (conventional grout and barium carbonate) were made for the sake of comparison.

1.2 OBJECTIVES

The objective of this research is to test the properties of grouts made with photon attenuating inclusions (barium carbonate and iron oxide). Compression strength, bleeding characteristics, and photon attenuation characteristics are the investigated properties of grouts used for post-tensioned concrete structures.

1.3 SUMMARY OF APPROACH

In order to achieve the objectives of this research, following tasks were completed:

1. The first task in this research was to perform compression strength tests on grouts made with various materials; barium carbonate ($BaCO_3$), iron oxide (Fe_2O_3), and Ottawa Sand. The strength test results for each type of grout were compared with conventional grout (Portland cement and water).

2. The second task in this research was to perform bleed tests on a grout mixture containing barium carbonate as well as cementitious grout.
3. The third task in this research was to perform radiography tests on grouts made with barium carbonate and compare the results with conventional grout.

1.4 SUMMARY OF FINDINGS

It was found that the compressive strengths of grouts made with either barium carbonate, iron oxide, or Ottawa Sand are higher than the minimum allowable strengths specified by the PTI. Moreover, although grouts made with barium carbonate exceeded the maximum permissible bleeding specified by the PTI, adding barium carbonate decreases the bleed water significantly compared to conventional grout. Finally, it was verified that adding $BaCO_3$ to grout increases its photon attenuation characteristics.

1.5 SCOPE OF REPORT

Chapter 2 provides background information related to this research. Information about grout, NDE, radiography, and $BaCO_3$ are presented in this section.

Chapter 3 presents the compressive strength tests. Included in this chapter is a description of the experimental program and variables treated, the experimental procedure and experimental results as well as a discussion of the results.

Chapter 4 presents the bleed tests. Both conventional grouts and grouts that include barium carbonate were included in the testing. The chapter describes the experimental procedure, experimental results, as well as a discussion of the results.

Chapter 5 presents the radiography tests. The tests included three different grout

mixtures as well as a concrete specimen. The chapter describes the experimental procedure, experimental results, as well as a discussion of the results.

Lastly, Chapter 6 summarizes the conclusions of this research and discusses future work needs related to this research topic.

CHAPTER 2

BACKGROUND

2.1 INTRODUCTION

This chapter reviews background information related to this research. Section 2.2 provides information about grout used in PT structures, and reviews the problems that sometimes arise with the grout during construction.

A brief description of the requirements for grout used in PT structures, as described in *Specification for Grouting of Post-Tensioned Structures* (PTI M55.1-12), hereafter referred to as PTI M55, which published by the PTI in 2012, is presented in this section. A brief overview of existing nondestructive evaluation methods to inspect grouted tendons in PT structures is presented in Section 2.3. Finally, Section 2.4 describes the concept of using photon attenuation inclusions within grout for PT structures.

2.2 GROUTS

In bonded PT structures, stressed strands are embedded in a duct and surrounded by grout. A typical cross section of a fully grouted tendon is shown in Figure 2.1. Grout is a cementitious material that fills the empty spaces in the tendon ducts not occupied by the prestressing steel.

Portland cement based grout has been used in the construction of the PT bridges in the US since the 1950's (Schupack, 2004). For PT structures, cementitious grout is usually composed of cement and water as well as admixtures essential to attain specific properties such as bleed resistance and fluidity (PTI, 2015).

Grout in bonded PT structures serves two primary functions: (1) providing corrosion protection to strands through its high alkalinity and the elimination of voids for water and other corrosion agents to come in contact with the prestressing steel; and, (2) providing a bond between the prestressing tendons and structure (Corven & Moreton, 2013). The performance and durability of strands are affected primarily by the quality of the surrounding grout. In particular, the incomplete grouting of the PT systems and the presence of voids within the hardened grout are the major problems encountered in the field (Azizinamini & Gull, 2012; Schupack, 2004). The severity of tendon corrosion is linked to the presence of grout voids, at which tendons are vulnerable to corrosion when water and oxygen (and possibly chlorides) are present (ACI, 2001; Schokker, Hamilton, & Schupack, 2002) . The formation of voids within grout also affects its ability to transfer bond between strands and surrounded concrete (Schokker, Breen, & Kreger, 2001).

In 1999, attention was paid to the durability of PT tendons in the US when some PT bridges were found to exhibit tendon failures (Theryo, Hartt, & Paczkowsk, 2013). For instance, Florida Department of Transportation (FDOT) discovered in 2000 a failed corroded tendon in one of the piers of its iconic bridge, the Sunshine Skyway Bridge, just thirteen years after being opened to traffic (FDOT, 2002). The presence of voids inside the PT ducts was one of the major causes for this failure (Trejo et al., 2009). Figure 2.2 shows the corroded tendon in the Sunshine Skyway Bridge (FDOT, 2002).

2.2.1 Overview of the PTI M55 Requirements

In response to the problems that were identified, many regulations were enacted regarding grout used in the PT structures to assure its quality as well as durability. Realizing the importance of the adequate grouting of the PT structures, the PTI in the US published PTI M55. This document provides minimum requirements for the selection, design, and installation of cementitious grout in PT construction. According to the Federal Highway Administration (FHWA), "Standard Specifications for Construction of Roads and Bridges on Federal Highway Projects (FP-14)," grout used in PT structures to fill void spaces inside ducts shall be in accordance with PTI M55.

A total of 9 laboratory tests are required by PTI M55 to be performed on the trial grout; they are as follows:

- Setting Time Test.
- Grout Strength Test.
- Permeability Test.
- Volume Change Test.
- Pumpability and Fluidity Tests.
- Bleed Tests.
- Corrosion Test.
- Wet Density Test.
- Inclined Tube Test.

In this research, only two of the above nine tests were performed on the investigated grouts; compressive strength test and bleed test. Because of the stiffening of grout made

with barium carbonate (explained in Section 3.5), all specimens in this research were batched using a water/cement ratio of 0.45, which is the maximum allowable ratio by PTI M55. Furthermore, PTI M55 requires that aggregates, if used, shall have a maximum size of 1 mm. Accordingly, the size of the Ottawa Sand used in this research is less than 0.84 mm.

2.2.2 Grout Strength Test

In order to perform its function in PT structures in terms of bonding, a minimum compression strength of grout shall be achieved (Ganz & Vildaer, 2002). PTI M55 specifies the minimum values for grout compression strength at ages 7 and 28 days to be 21 and 35 MPa, respectively. Moreover, PTI M55 requires that grout strength test must be determined, using cube specimens, in accordance with ASTM C942, *Standard Test Method for Compressive Strength of Grouts for Preplaced-Aggregate Concrete in the Laboratory*. Accordingly, grout compression strength tests in this research were prepared and tested, generally, following the requirements of ASTM C942. Minor deviations from the ASTM requirements were made regarding specimen storing, temperature, and specimens testing ages.

ASTM C942 requires that specimens shall be stored in a moist room or moist closet immediately upon completion of molding for a duration of 20 to 72 h. In this research, there was no moist room; rather, plastic sheeting was used to cover specimens.

Concerning temperature, ASTM C942 requires that the temperature of the air in the vicinity of the mixing slab, the dry materials, molds, and mixing bowl, shall be maintained between 23 ± 3°C. Furthermore, the temperature of the mixing water, moist closet or moist

room, and water in the water bath shall be set at 23 ± 2°C. The laboratory used to conduct the research does not have precise temperature control, but the observed room temperature generally was around 24°C. In this research, all mixing tools and dry materials as well as mixing water and water in the water bath were prepared and set in the laboratory one day prior to mixing to allow all tools and materials to reach thermal equilibrium with the laboratory. For the first 12 hours after casting, after which the specimens (still in the molds) were immersed in a lime-saturated water bath.

Finally, although PTI M55 specifies two ages at which grouts must achieve minimum values, an additional test at an age of 3 days was included in this research to provide more information about early age strength gain.

2.2.3 Bleed Test

Bleeding is the segregation of solid particles of grout from water due to differences in density (Newman & Choo, 2003; Schupack, 2004). After the grout is placed, the denser particles such as cement settle down due to gravity, displacing less dense material such as water to the top. Inside a duct, this bleed water can migrate to the inside top surface of the duct and produce voids at which the strands will be vulnerable to corrosion. Moreover, large void formations in the post-tensioning duct can decrease the bond between the tendon and the concrete section.

Grout bleeding is considered one of the most significant factors that affect the durability of grout (Ganz & Vildaer, 2002). (Trejo et al., 2009) mentioned that one of the factors that led to the tendon failure in the Sunshine Skyway Bridge was the formation of voids inside the PT ducts, especially near the anchorage zones, resulting from bleed water

evaporation. Consequently, grout must be bleeding resistant to increase its quality (Schokker et al., 2002).

Two types of bleed tests are required by PTI M55; wick-induced bleed test and Schupack pressure bleed test. In this research, all performed bleed tests were wick-induced bleed tests.

According to PTI M55, a modification of the ASTM C940 test, *Standard Test Method for Expansion and Bleeding of Freshly Mixed Grouts for Preplaced-Aggregate Concrete in the Laboratory*, shall be used to assess the grout. PTI M55 requires that the testing device shall consist of a transparent tube and have the following approximate dimensions: height of 1000 mm and internal nominal diameter of 80 mm. Moreover, PTI M55 requires that maximum bleed water at the end of the three hours shall be 0.0%. Some deviations from the ASTM requirements were made regarding recording times.

Although PTI M55 requires that bleeding must be recorded for three hours, recordings in this research were taken up to two hours. The reason of that is because the objective of the test was to compare conventional grout with grout made with barium carbonate, and the bleeding of the barium carbonate grouts stabilized after 2 hours. Moreover, PTI M55 requires that bleed water must be measured every 15 minutes for the first hour, and then hourly afterward. Measurements in this research were taken every 15 minutes for the entire two hours in order to obtain additional information.

Assaad, Daou, & Harb (2015) showed that the wick-induced bleeding increases proportionally to the water/cement ratio.

2.3 NON-DESTRUCTIVE EVALUATION OF GROUT

Inspection for grout voids or prestressing steel corrosion is difficult in bonded PT structures. Grout voids or steel corrosion are located inside the duct which in most instances (but not always) is embedded in the concrete section.

One method to inspect for voids involves drilling a hole into the section to visually inspect for a void using a borescope (Corven & Moreton, 2013). That method works only if the drilled hole intersects the void.

As an alternative to drilling a hole (or to guide where to drill the hole), various methods have been researched to non-destructive inspect for grout voids or corrosion. A recent ATLSS report (1015) by Cercone, Naito, Corven, Pessiki, Keller, and Pakzad titled "*Designing and Detailing Post Tensioned Bridges to Accommodate Non-Destructive Evaluation*" (hereafter referred to as the ATLSS NDE report) reviews several NDE methods and their useful use for grout void and corrosion detection in PT structures.

Methods reviewed in the report include:

- Acoustic Emission.
- Electrically Isolated Tendons.
- Ground Penetrating Radar.
- Half-Cell Potential.
- Impact Echo.
- Infrared Thermography.
- Magnetic Flux Leakage.
- Radiography.
- Time Domain Reflectometry.

- Ultrasonic Testing.
- Visual Inspection.

Further details related to the applications, methodology, limitations, and viability of each method in PT applications are presented in the ATLSS NDE report.

One method in particular is relevant to the work presented in this report, namely radiography. The following section reviews the application of radiography for the inspection of PT structures. The information presented is taken directly from the ATLSS NDE report.

2.3.1 Radiography

Applications

Radiography has been used to detect grout voids, strand corrosion, and strand fracture in the tendons of PT concrete bridges (Mariscotti, Jalinoos, Frigerio, Ruffolo, & Thieberger, 2008; Pimentel et al., 2010; Saravanan et al., 1996). In addition, this method has been utilized for the verification of re-grouting operations, the location and sizing of steel reinforcing bars and embedded utilities, and the visualization of unknown construction details (Brown & St Leger, 2003). Radiography accommodates a wide range of construction materials (including plastic and metal ducts), embedded features with complex geometries, and both internal and external post-tensioning configurations (Pimentel et al., 2010; Saravanan et al., 1996). Access to the front and back surfaces of the scanned region is required.

The recent development of portable high intensity Megaelectron volts (MeV) x-ray generators (Figure 2.3) now enable the inspection of concrete sections up to 150 cm thick

(Uesaka, Jin, Wu, & Dobashi, 2013; Sentinel, 2014). Unlike gamma ray-producing isotope sources, these portable x-ray machines only emit radiation during testing, thereby providing better control over work site safety. The use of high intensity x-rays has also reduced the required transmission time so that radiographic images with sufficient detail for defect/damage detection can be generated in a matter of seconds. For example, Uesaka et al. (2013) were able to generate radiographic images of a 400 mm thick PT bridge section with transmission times of one second using a newly developed 3.95 MeV portable x-ray generator.

Methodology

Radiography utilizes the electromagnetic waves emitted from a radiation source (either an x-ray generator or a radio isotope gamma-ray source) to penetrate the test object, exposing a photostimulable detector on the opposing surface. Since the atomic structure of the surveyed material influences photon attenuation and scattering phenomena, spatial variation in material composition leads to spatial variation in radiation intensity reaching the detector (as illustrated in Figure 2.4). In modern digital radiographic testing, these detector readings are digitized and converted to pixel intensity values, through which spatial variations can be visualized on a computer monitor as color contrast. In NDE applications, this spatial variation in pixel intensity is used to identify and measure defects or structural damage, and to visualize embedded features for repair/retrofit operations. As a practical illustration, Figure 2.5 presents radiographs of fully grouted and voided post-tensioning tendons, where the voided duct region is discernible in the image (shown as a darker region due to higher incident radiation).

The ability of radiographic imaging to accommodate complex geometries and multi-layer material interfaces (which present problems for other nondestructive test methods), and to provide full-field subsurface visualization make it a powerful tool for structural condition assessment. However, its use in concrete bridge inspection has historically been limited by the penetrating power of field deployable radiation sources, as well as safety and logistical concerns associated with the use and transport of radioactive materials. Recent advances in radiographic inspection equipment, such as the development of portable high intensity MeV x-ray generators (discussed in the previous section); now enable the inspection of concrete sections up to 150 cm thick with transmission times on the order of seconds (Uesaka et al., 2013; Sentinel, 2014). Unlike gamma ray-producing isotope sources, these portable x-ray machines only emit radiation during testing, thereby providing better control over work site safety. In addition, the development of digital detectors and advanced image reconstruction algorithms for concrete materials that reduce scatter-induced blurring (e.g. (Priyada, Ramar, & Shivaramu, 2013)) have improved imaging capabilities, and have enhanced data preservation and manipulation. As an illustration, Figure 2.6 presents a radiograph of a post-tensioning anchorage region showing individual steel strands, the reinforcing steel spiral (encircling the duct), and the tendon duct.

Limitations

Due to the procedure's use of radioactive materials in certain applications, radiography may require special preparations and planning to ensure public safety. It is noted that certain site conditions may prohibit this type of testing, but instrumentation such

as x-ray generators exist where radioactive material is not used. In addition, conventional methods for radiographic imaging do not provide depth of field information for the surveyed structure, although the development of portable x-ray generators has initiated research interest in adapting advanced 3-D imaging techniques, e.g. computed tomography (CT), to structural inspection. The use of radiography also requires access to opposing sides of the surveyed object.

Viability in Post-Tensioned Applications

Radiography is an imaging tool that can be used to detect and quantify subsurface features/defects in PT concrete bridges. The testing procedure is able to handle complex geometries and multi-layer material interfaces, which can present problems for other NDE methods and therefore can be a viable tool when a more in-depth inspection of the strand anchorage and coupler regions is required. With further development and verification, radiography could potentially identify corrosion on strands and grout voids. Newly developed portable high intensity MeV x-ray machines, which can survey concrete bridge sections up to 150 cm thick with transmission times on the order of seconds, have improved the efficiency, practicality, and imaging capabilities of radiographic testing (Uesaka et al., 2013). In addition, advanced digital image analysis methods (e.g. Priyada et al., 2013) have improved defect/damage detection capabilities.

2.3.2 Overview of Some Terminology Related to Radiography Tests

Optical Density:

The optical density measurements of a film depend on number of photons that passed through imaged object and captured by the radiation sensitive film. Higher optical density (i.e. a darker film) comes from greater exposure of the film. A void would show up as a darker region because the absence of material would result in greater exposure of the film.

Exposure Time:

The exposure time is the time during which the object is being radiographed. As the exposure time increases, the film becomes darker. Therefore, higher optical density measurements would result from increased exposure times.

2.4 PHOTON ATTENUATING INCLUSIONS

As mentioned previously, the ability of radiographic imaging to accommodate complex geometries as well as multi-material composite structures makes it an efficient tool in assessing the subsurface zones (Keller & Pessiki, 2016). Despite that, the similarity in photon attenuation between cementitious grout and surrounding concrete makes it difficult to distinguish small voids in a thick concrete section in radiographic imaging (Keller & Pessiki, 2016). This difficulty increases at anchorages zones because of complexity, congested reinforcing steel, closely spaced tendon ducts, and variable concrete thickness which is of the main challenges encountered in NDE (Limaye & Kakade, 2008).

Keller & Pessiki (2016) investigated the use of cementitious grout materials with the addition of photon attenuating inclusions (PAI) in order to improve radiographic

visualization. PAI are defined as high atomic number materials, possessing advantageous radiation attenuation properties, which are embedded within the parent material for the purpose of altering its radiation attenuation characteristics. The fundamental concept is that PAI can be used to tune radiation attenuation in the component materials of a composite structure (with regard to both material attenuation characteristics and the radiation emission spectrum) in order to improve contrast in radiographic images. Keller & Pessiki (2016) investigated three candidate PAI materials in their study: (1) iron (Fe); (2) barium carbonate ($BaCO_3$); and, (3) barium sulfate ($BaSO_4$).

Keller & Pessiki (2016) explained that the barium compound grouts investigated in the study were of primary interest since barium has a K-edge around 37 keV. Near this energy level, there is a sudden increase in photoelectric absorption of photons just above the binding energy of the K shell electrons. As illustrated in Figure 2.7, this sudden increase in attenuation at the K-edge has a significant influence on the attenuation spectrum between 37-300 keV. Iron has a K-edge around 7 keV and therefore impacts attenuation over a lower energy region of the spectrum, much of which is effectively filtered during imaging of thicker structural concrete sections.

Keller & Pessiki (2016) explained that at higher energy levels, such as those employed by MeV x-ray betatrons (1-9 MeV), attenuation in all materials is relatively low and mainly due to Compton scattering, i.e. the influence of photoelectric absorption is significantly reduced. For high atomic number elements such as barium, however, a second form of attenuation in this higher energy region of the emission spectrum known as pair production becomes significant. The probability of pair production increases with photon energy and atomic number of the element interacting with the photon.

The pre-packaged base grout material used in the study by Keller and Pessiki consisted of cement, water, and sand. Specimens were exposed to 350 keV of radiation for 480 seconds. The optical density measurements were taken along the x-axis of the diameter of the specimen as shown in Figure 2.8. The optical density measurements of the radiographic images generated for the base and PAI grout specimens, which were 30 cm thick, are presented in Figure 2.9, along with an additional measurement for a Portland cement concrete specimen. It can be seen that radiation attenuation in cementitious grout can be significantly increased with iron and barium compound inclusions with a note that both barium carbonate and barium sulfate had close results and were stronger attenuators than iron.

Based on previous results (taken from Keller & Pessiki (2016)), barium carbonate and iron oxide as well as Ottawa Sand, which was included in the pre-packaged base grout, are investigated in this research.

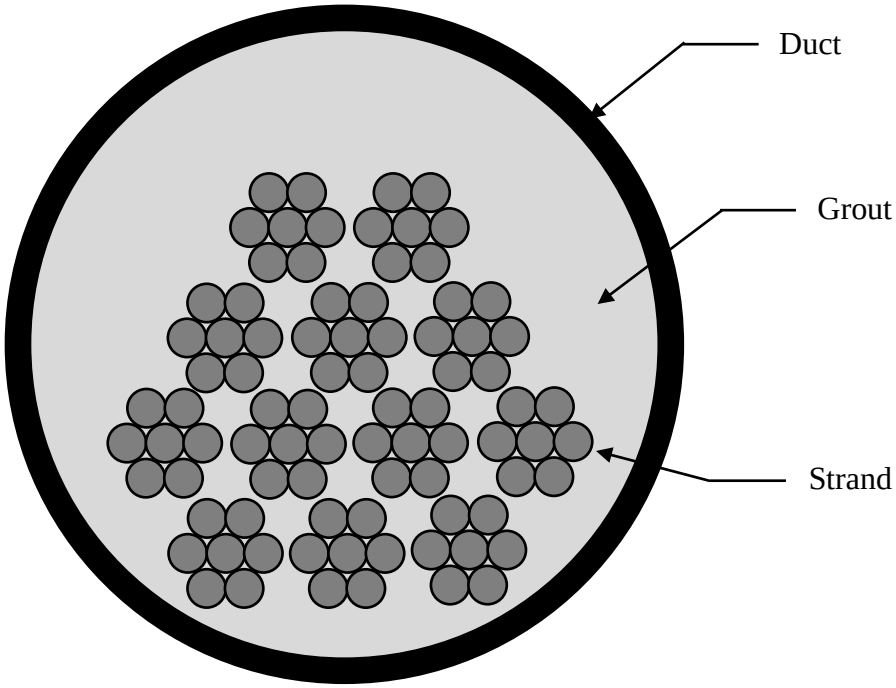

Figure 2.1 - Typical cross section of a fully grouted tendon.

Figure 2.2 - Corroded tendon in the Sunshine Skyway Bridge (FDOT, 2002).

Figure 2.3 - Portable 7.5MeV X-ray Betatron (www.Sentinelndt.com).

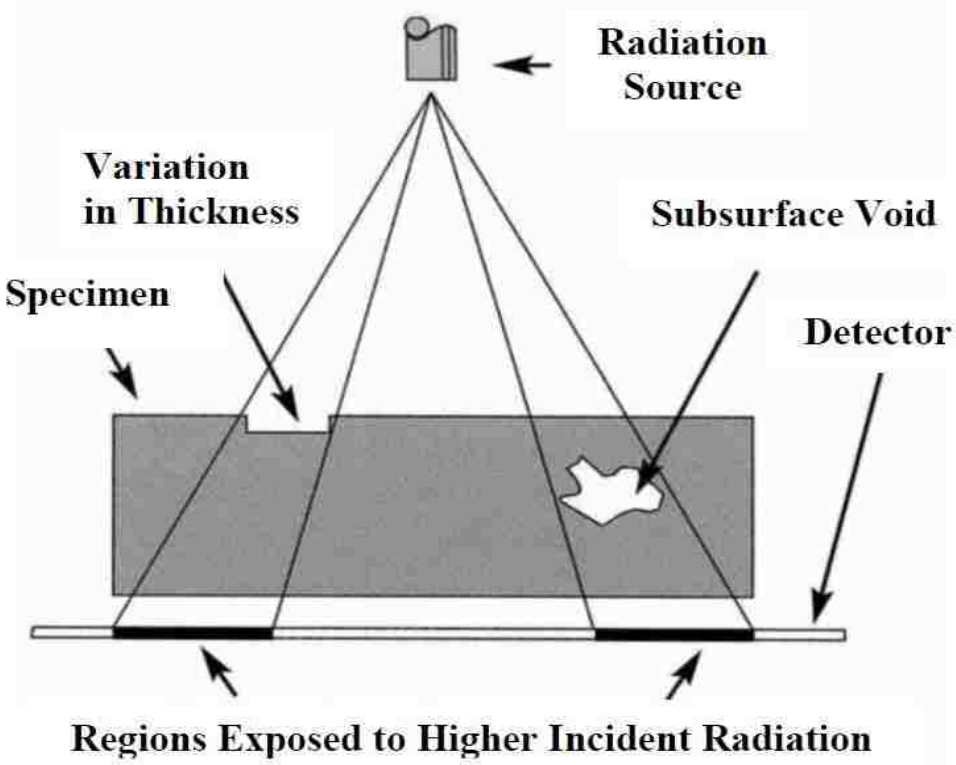

Figure 2.4 - Schematic illustration of radiographic testing (ATLSS NDE report, 2015).

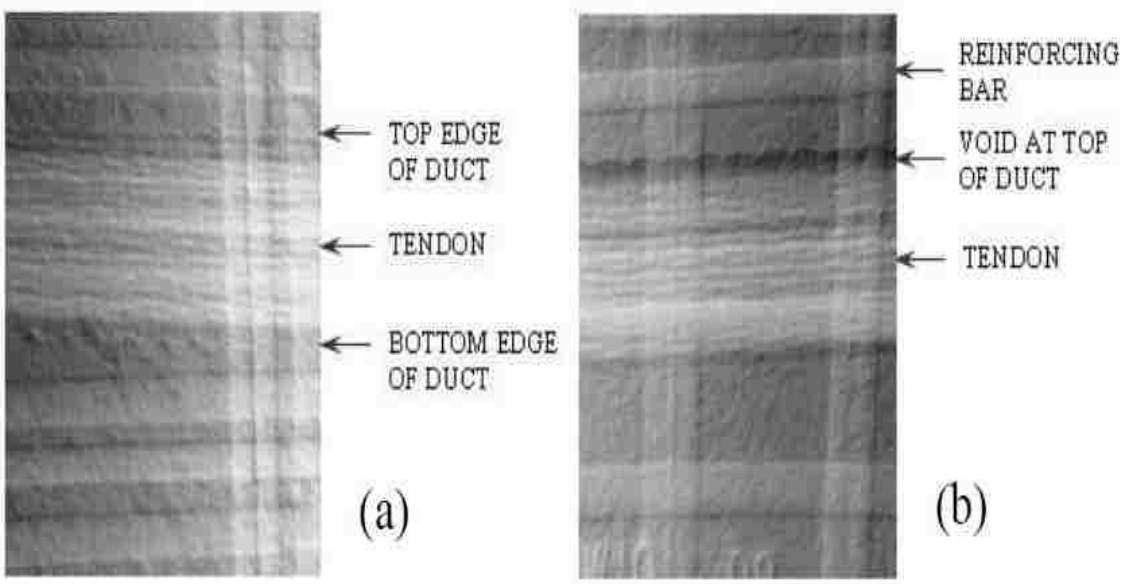

Figure 2.5 - Radiographic images of post-tensioned concrete: (a) fully grouted post-tensioning steel duct, (b) voided post-tensioning steel duct (Brown & St Leger, 2003).

Figure 2.6 - Radiograph of the anchorage region in a post-tensioned concrete bridge showing individual strands, the reinforcing steel spiral (encircling the duct), and the tendon duct (Washer, 2003).

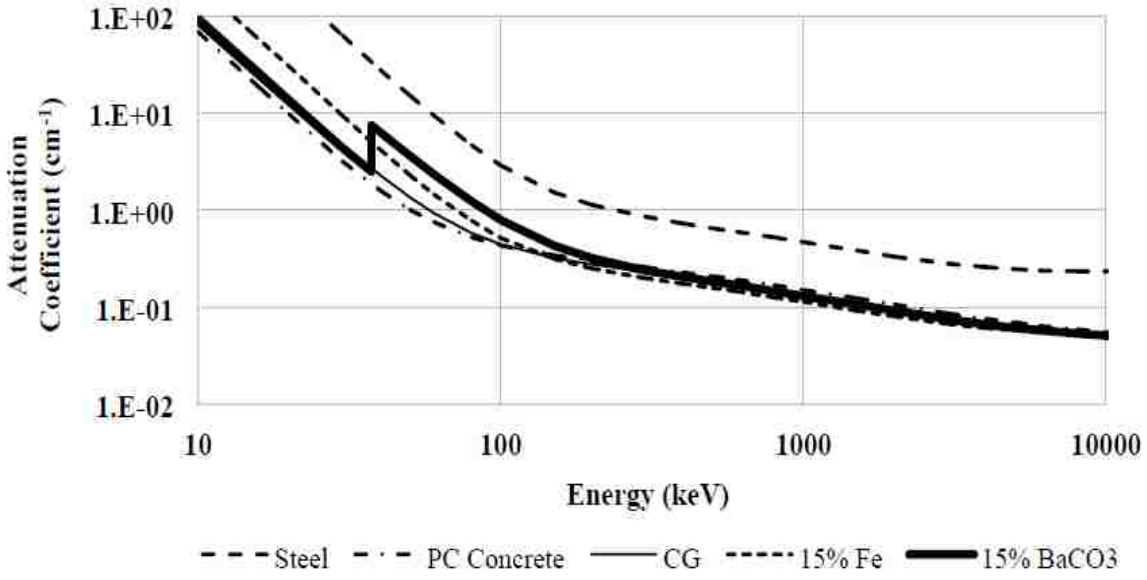

Figure 2.7 - Attenuation coefficients (Keller & Pessiki, 2016).

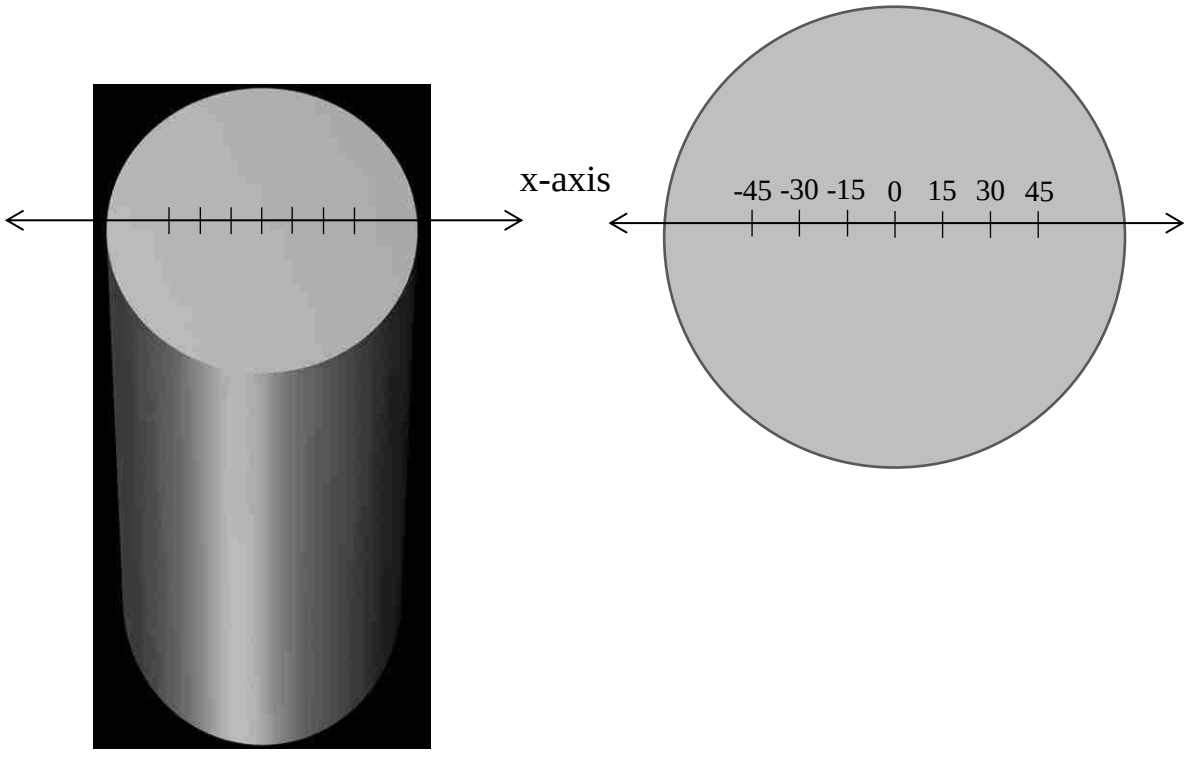

Figure 2.8 - Keller and Pessiki (2016) measured optical density for all specimens along x-axis.

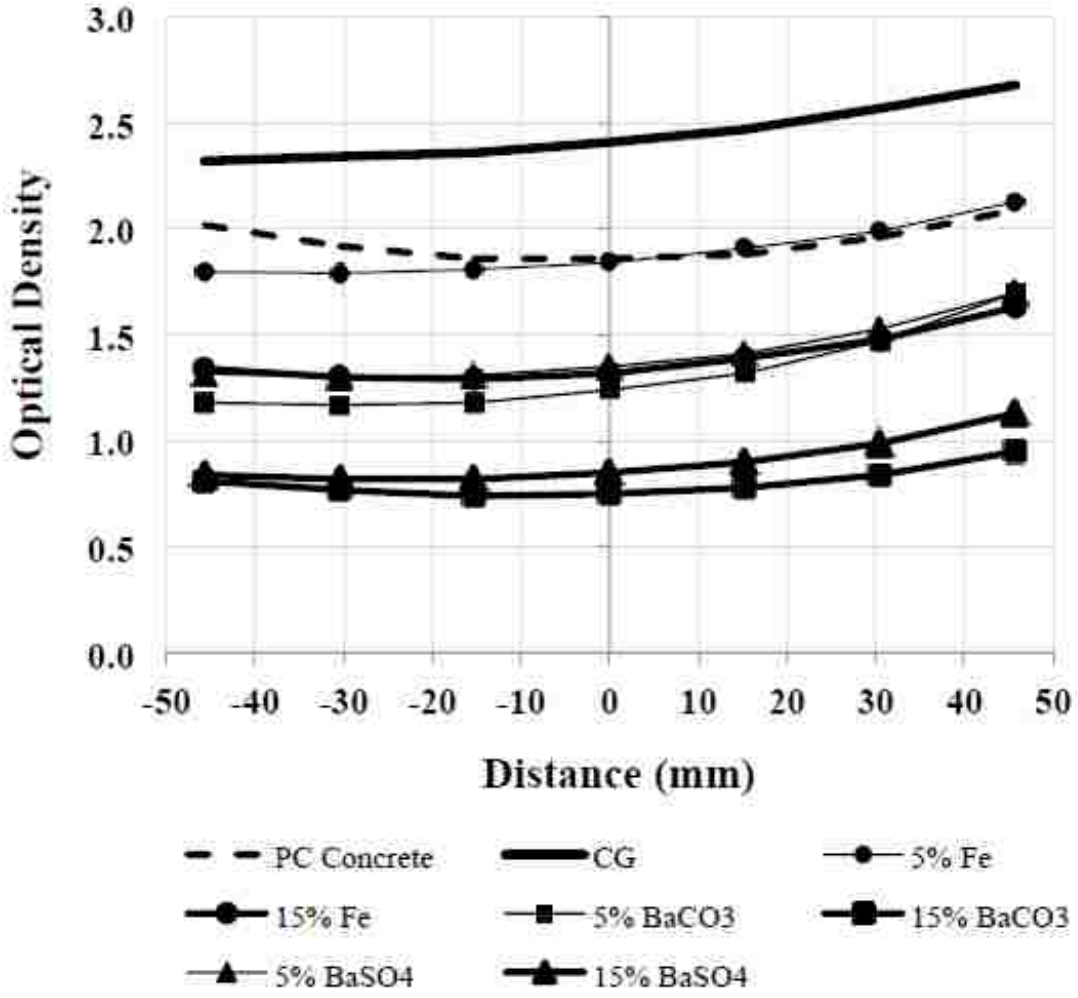

Figure 2.9 - Optical density measurements for 30 cm thick grout specimens with and without PAI "350 keV-12.85 mA-480 s-Agfa D4 film"
(adapted from Keller & Pessiki, 2016).

CHAPTER 3

COMPRESSIVE STRENGTH TESTS

3.1 INTRODUCTION

This chapter presents the compressive strength tests. A description of the experimental program is provided in Section 3.2. This includes a description of the test matrix, specimen mixture proportions, as well as details of specimens preparation and testing. After that, Section 3.3 presents the experimental results of all specimens. Next, a discussion of these results is presented in Section 3.4. Finally, the conclusions of this chapter are presented in Section 3.5.

3.2 DESCRIPTION OF EXPERIMENTAL PROGRAM

3.2.1 Test Matrix

The test matrix for the grout compressive strength tests is shown in Table 3.1. As shown in the table, six different groups of specimens were tested (CG, B10, B20, F10, F20, and OS). CG refers to the specimens that were conventional grout, made with only Type I Portland cement and water. B10 and B20 refer to specimens made with 10% and 20% by weight barium carbonate ($BaCO_3$), respectively. Similarly, F10 and F20 refer to specimens made with 10% and 20% by weight iron oxide (Fe_2O_3), respectively. Finally, OS refers to specimens made with Ottawa Sand.

A total of 12 different mixtures were batched, denoted with the 12 Specimen ID notations given in Table 3.1. Each replicate batch is given a numeric identifier. For example, the two batches of conventional grout are identified as CG.1 and CG.2.

3.2.2 Mixture Proportions

Mixture proportions of all specimens are shown in Table 3.2. As shown in the table, 12 different grout batches were tested. A total of 9 50-mm cube specimens were prepared from each batch. The water/cement ratio for all batches was fixed at 0.45. In order to ensure the adequacy of the quantity of the mixing materials, 2000 cm^3 were mixed for each batch.

3.2.3 Specimen Preparation

All mixing tools and dry materials as well as mixing water and water in the water bath were prepared and set in the laboratory one day prior to mixing to assure that all materials were at the same temperature. On the day of mixing, all ingredients were mixed using a benchtop mixer as follows: the dry ingredients were mixed manually first to make certain they were well blended. Then, the water was added to the mixer. After that, the dry ingredients were added gradually to the mixer within 2 minutes. Materials were mixed for additional 0.5 minutes to assure their uniformity. After that, the mixer was paused for 1 minute to scrape down into the bowl any material stuck on its side. Finally, materials were mixed again for 2.5 minutes. Figure 3.1 shows materials during the mixing process.

Three molds, with three cube compartments for each, were prepared for each batch. Before placing grout inside them and in accordance with the ASTM C109/C109M, the molds surfaces were cleaned and greased using a rag prior to grout placement to facilitate removal of the cured cubes from the molds. After completion of mixing, grout was placed in the molds with two layers; each is about 25 mm (half of depth of the mold). Each layer of each cube was tamped 16 times in 2 rounds; each round was at right angles to the other. Finally, a trowel was used to finish specimens surfaces with a sawing motion across the

top of each mold. Molds filled with grout are shown in Figure 3.2.

As mentioned in Section 2.2.1, a deviation from ASTM C942 was made regarding curing the specimens. ASTM C942 requires that test specimens shall be placed in a moist room immediately upon completion of molding. Rather in this research, one hour after the start of mixing, the specimens were covered with wet plastic sheeting to reduce evaporation of water as shown in Figure 3.3. Specimens remained covered with the plastic sheet until they reached the age of 12 hours, and then they were immersed in a lime-saturated water bath. When specimens were at an age of 24 hours, they were removed from the molds and immediately returned to the water bath until they were tested in compression. Figure 3.4 shows the water bath filled with stripped specimens as well as those still in molds.

3.2.4 Specimen Testing

Each batch was tested at three different ages; 3, 7, and 28 days with a total of 3 cubes for each test. To perform a strength test, each cube was removed from its water bath, and its surfaces were wiped to a surface-dry condition. Each cube was then placed in the compression testing machine with two formed co-planar surfaces against the machine platens. Specimens were loaded within a range of 900 to 1800 N/s. A photograph of the machine used to compress specimens is shown in Figure 3.5.

3.3 EXPERIMENTAL RESULTS

The experimental results are presented in this section. Section 3.3.1 presents the results for the conventional grout specimens. Results for grouts made with barium carbonate are presented in Sections 3.3.2 and 3.3.3. Sections 3.3.4 and 3.3.5 present the

results for grouts made with iron oxide. Finally, Section 3.3.6 presents the results for the grout made with Ottawa Sand. In each section, a table showing complete results as well as their averages is presented, followed by a figure showing a plot of the results.

All compressive strength results are rounded to nearest 0.1 MPa, as specified in the ASTM C942.

3.3.1 Grout CG (CG.1 and CG.2)

Two replicate batches of conventional grout (CG.1 and CG.2) were made on two different days and tested in compression at ages 3, 7, and 28 days. The compressive strength results of these two specimens and their averages are tabulated in Table 3.3. Figure 3.6 is a plot of the compression strength of each cube test for the two batches of CG Specimens.

3.3.2 Grout B10 (B10.1 and B10.2)

Two batches of B10 (B10.1 and B10.2), which had Portland Type I cement, water, and barium carbonate, were made on two different days and tested in compression at ages 3, 7, and 28 days. The amount of barium carbonate used in each specimen was 10% of cement weight. Table 3.4 presents the compressive strength results of these two specimens as well as their averages. Figure 3.7 is a plot of the compression strength of each cube test for the two batches of B10 Specimens. The low average compressive strength of Specimen B10.2 at age 7 days, as compared to Specimen B10.1, is affected by the weak result of the third cube.

3.3.3 Grout B20 (B20.1 and B20.2)

Two batches of B20 (B20.1 and B20.2), which had Portland Type I cement, water, and barium carbonate, were made on two different days and tested in compression at ages 3, 7, and 28 days. The amount of barium carbonate used in each specimen was 20% of cement weight. Table 3.5 presents the compressive strength results of these two specimens as well as their averages. Figure 3.8 is a plot of the compression strength of each cube test for the two batches of B20 Specimens.

3.3.4 Grout F10 (F10.1 and F10.2)

Two batches of F10 (F10.1 and F10.2), which had Portland Type I cement, water, and iron oxide, were made on two different days and tested in compression at ages 3, 7, and 28 days. The amount of iron oxide used in each specimen was 10% of cement weight. Table 3.6 presents the compressive strength results of these two specimens as well as their averages. Figure 3.9 is a plot of the compression strength of each cube test for the two batches of F10 Specimens.

3.3.5 Grout F20 (F20.1 and F20.2)

Two batches of F20 (F20.1 and F20.2), which had Portland Type I cement, water, and iron oxide, were made on two different days and tested in compression at ages 3, 7, and 28 days. The amount of iron oxide used in each specimen was 20% of cement weight. Table 3.7 presents the compressive strength results of these two specimens as well as their averages. Figure 3.10 is a plot of the compression strength of each cube test for the two batches of F20 Specimens.

3.3.6 Grout OS (OS.1 and OS.2)

Two batches of OS (OS.1 and OS.2), which had Portland Type I cement, water, and Ottawa Sand, were made on two different days and tested in compression at ages 3, 7, and 28 days. The amount of Ottawa Sand used in each specimen was 20% of cement weight. Table 3.8 presents the compressive strength results of these two specimens as well as their averages. Figure 3.11 is a plot of the compression strength of each cube test for the two batches of OS Specimens.

3.4 DISCUSSION OF GROUT STRENGTH TEST RESULTS

The compression strength test results presented in previous section are discussed and analyzed in this section. The discussion focuses on three aspects of the results: (1) average compressive strength values; (2) required compression strength values; and (3) the effect of barium carbonate, iron oxide, and Ottawa Sand on grout compressive strength.

3.4.1 Average Compressive Strengths of all Specimens

Table 3.9 presents the average compressive strengths of all specimens at ages 3, 7, and 28 days. Moreover, the same results are plotted in Figure 3.12. It can be clearly seen that at the ages of 3 and 7 days, all specimens have similar strengths except Specimen B10 which has lower compressive strengths at both ages. On the other hand, compressive strength results of all specimens at age 28 days are close to each other with a note that grouts having sand and 10% iron oxide have the highest strength results. Moreover, it is noted that the average compressive strength of Specimen B10 increased from 36.8 MPa at age 7 days to 46.7 MPa at age 28 days with about 26.9% increasing while Specimen B20

increased about 11.7% for the same interval. Similarly, the strength of Specimen F10 increased from 39.9 MPa at age 7 days to be 49.6 MPa at age 28 days with an increasing of about 24.3%, whereas it increased about 10.7% for Specimen F20.

3.4.2 Comparing Averages to the Required Results

As explained in Chapter 2, PTI M55 requires that grout used in PT structures shall meet minimum strengths of 21 MPa and 35 MPa at ages 7 and 28 days, respectively. In order to compare the average compressive strengths obtained in the preceding section to the required minimum results, all results have been normalized to the minimum required results (denoted by R) at ages 7 and 28 days and presented in Table 3.10. Moreover, Figure 3.13 shows the average compressive strengths of all specimens normalized by the required result at each age. It can be clearly seen that all specimens have achieved the required strengths at both ages 7 and 28 days. Furthermore, Figure 3.13 shows that the differences between required and achieved results at age 7 days are higher than at age 28 days for all specimens.

3.4.3 Effect of Barium Carbonate, Iron Oxide, and Ottawa Sand on Grout Compression Strength

The effect of barium carbonate on grout strength, compared with conventional grout, is discussed first. After that, the effect of iron oxide and Ottawa Sand, compared to conventional grout, is discussed in two separate sections. For each comparison, two graphs are presented. The first graph shows the strength values, while the second graph presents strength results normalized by the conventional grout at each age.

Barium Carbonate

Figure 3.14(a) shows the average compressive strengths of the conventional grout as well as specimens having barium carbonate, at ages 3, 7, and 28 days, while Figure 3.14(b) presents these results normalized by the conventional grout results. It is noted that at ages 3 and 7 days, grouts containing barium carbonate are weaker than the conventional grout with a note that the differences between the two types of grouts are smaller at later ages. In other words, Specimen B10 is weaker than Specimen CG by 18% at an age of 3 days and 13% at an age of 7 days. The B20 Specimen is 6% weaker than the CG Specimen at an age of 3 days and 3% at an age of 7 days. On the other hand, specimens at age 28 days have very close results with a note that grout made with 10% barium carbonate is slightly stronger than other two specimens by about 2%. For both Specimens B10 and B20, Figure 3.14 shows that as the age of specimens increases, their average compressive strengths approach to the conventional grout strength. Moreover, although Specimen B20 is stronger than B10 at ages 3 and 7 days by about 14.6% and 11.7%, respectively, Specimen B10 is slightly stronger at the age of 28 days by about 1.7%. Although it is noted that there is no clear pattern describing the relation between increasing barium carbonate within grout and its strength, adding barium carbonate neither weakened the grout at age 28 days nor violated the minimum requirements of PTI M55.

Iron Oxide

Figure 3.15 (a) shows the average compressive strengths of the conventional grout as well as specimens having iron oxide, at ages 3, 7, and 28 days, while Figure 3.15(b) presents these results normalized by the conventional grout results. It is noted that at an age of 3 days, grouts made with iron oxide are weaker than the conventional grout with a

note that Specimen F20 is 4% weaker than Specimen F10. On the other hand, the strength of Specimen F20 at an age of 7 days is almost equal to the conventional grout while Specimen F10 is weaker by 6%. At 28 days age, both Specimens F10 and F20 are stronger than the conventional grout by about 8.3% and 3.5%, respectively. Although it is noted that there is no clear pattern describing the relation between increasing iron oxide within grout and its strength, adding iron oxide neither weakened the grout at age 28 days nor violated the minimum requirements of PTI M55.

Ottawa Sand

Figure 3.16(a) shows the average compressive strengths of the conventional grout as well as specimens made with Ottawa Sand, at ages 3, 7, and 28 days, while Figure 3.16(b) presents these results normalized by the conventional grout results. It is noted that at an age of 3 days, the strength of grouts containing Ottawa Sand is almost equal to the conventional grout. On the other hand, the strength of Specimen OS at an age of 7 days is weaker than the conventional grout by 5.2%. At 28 days age, Specimen OS is stronger than the conventional grout by about 8.7%.

3.5 ADDITIONAL OBSERVATIONS FROM GROUT COMPRESSION TESTS

It was observed that adding barium carbonate to the grout increased its stiffness as compared to the conventional grout consisting of cement and water. Accordingly, no specimen was made with barium carbonate comprising more than 20% of the weight of cement.

3.6 CONCLUSIONS FROM GROUT COMPRESSION TESTS

The following conclusions are drawn from the grout compression tests:

1. Adding barium carbonate to grout did not have an adverse effect on its compression strength.
2. All grout specimens made with barium carbonate satisfied the minimum strength requirements of PTI M55. At the age of 3 and 7 days, the strength of the barium carbonate grouts were slightly lower than the strength of the conventional grout.
3. Adding iron oxide to grout did not have an adverse effect on its compression strength.
4. All grout specimens made with iron oxide satisfied the minimum strength requirements of PTI M55. At the age of 3 days, the strength of the iron oxide grouts was slightly lower than the strength of the conventional grout.
5. Adding Ottawa Sand, which was used by Keller & Pessiki (2016) within conventional grout components, to grout did not have an adverse effect on its compressive strength. Rather, the highest result was achieved by Specimen OS at an age of 28 days.
6. All grout specimens made with Ottawa Sand satisfied the minimum strength requirements of PTI M55. At the age of 3 and 7 days, the strength of the Ottawa Sand grouts were slightly lower than the strength of the conventional grout.

Table 3.1 - Compressive strength test matrix.

Group	Mix ID	Comments
CG	**CG.1**	**Type I Portland cement + water**
	CG.2	
B10	**B10.1**	**Type I Portland cement + 10% barium carbonate (by weight) + water**
	B10.2	
B20	**B20.1**	**Type I Portland cement + 20% barium carbonate (by weight) + water**
	B20.2	
F10	**F10.1**	**Type I Portland cement + 10% iron oxide (by weight) + water**
	F10.2	
F20	**F20.1**	**Type I Portland cement + 20% iron oxide (by weight) + water**
	F20.2	
OS	**OS.1**	**Type I Portland cement + 10% Ottawa Sand (by weight) + water**
	OS.2	

Table 3.2 - Mixture proportions for compressive strength test.

Mix ID	Mixture Proportions (grams)					Comments
	Cement	Water	$BaCO_3$	Fe_2O_3	Ottawa Sand	
CG.1	2606	1173	0	0	0	Conventional grout (cement + water)
CG.2	2606	1173	0	0	0	
B10.1	2529	1138	253	0	0	10% barium carbonate (by weight)
B10.2	2529	1138	253	0	0	
B20.1	2457	1106	491.5	0	0	20% barium carbonate (by weight)
B20.2	2457	1106	491.5	0	0	
F10.1	2543	1144	0	254	0	10% iron oxide (by weight)
F10.2	2543	1144	0	254	0	
F20.1	2483	1117	0	497	0	20% iron oxide (by weight)
F20.2	2483	1117	0	497	0	
OS.1	2484	1118	0	0	248	10% Ottawa Sand (by weight)
OS.2	2484	1118	0	0	248	

Figure 3.1 - Photograph of benchtop mixer.

Figure 3.2 - Photograph of 9 50-mm grout cube specimens after molding.

Figure 3.3 - Photograph of grout specimens covered with wet plastic sheeting prior to wet-curing.

Figure 3.4 - Photograph of specimens immersed in a lime-saturated water bath for curing.

Figure 3.5 - Photograph of compression testing machine.

Table 3.3 - Compressive strength results of Specimens CG.1 and CG.2.

Mix ID	Age at Test (days)	Compressive Strength (MPa)			Average Compressive Strength (MPa)
CG.1	3	36.5	38.1	36.0	36.9
	7	39.4	39.2	40.8	39.8
	28	41.3	42.7	45.4	43.1
CG.2	3	39.6	41.7	43.4	41.5
	7	46.7	42.4	46.2	45.1
	28	43.7	53.0	48.5	48.4

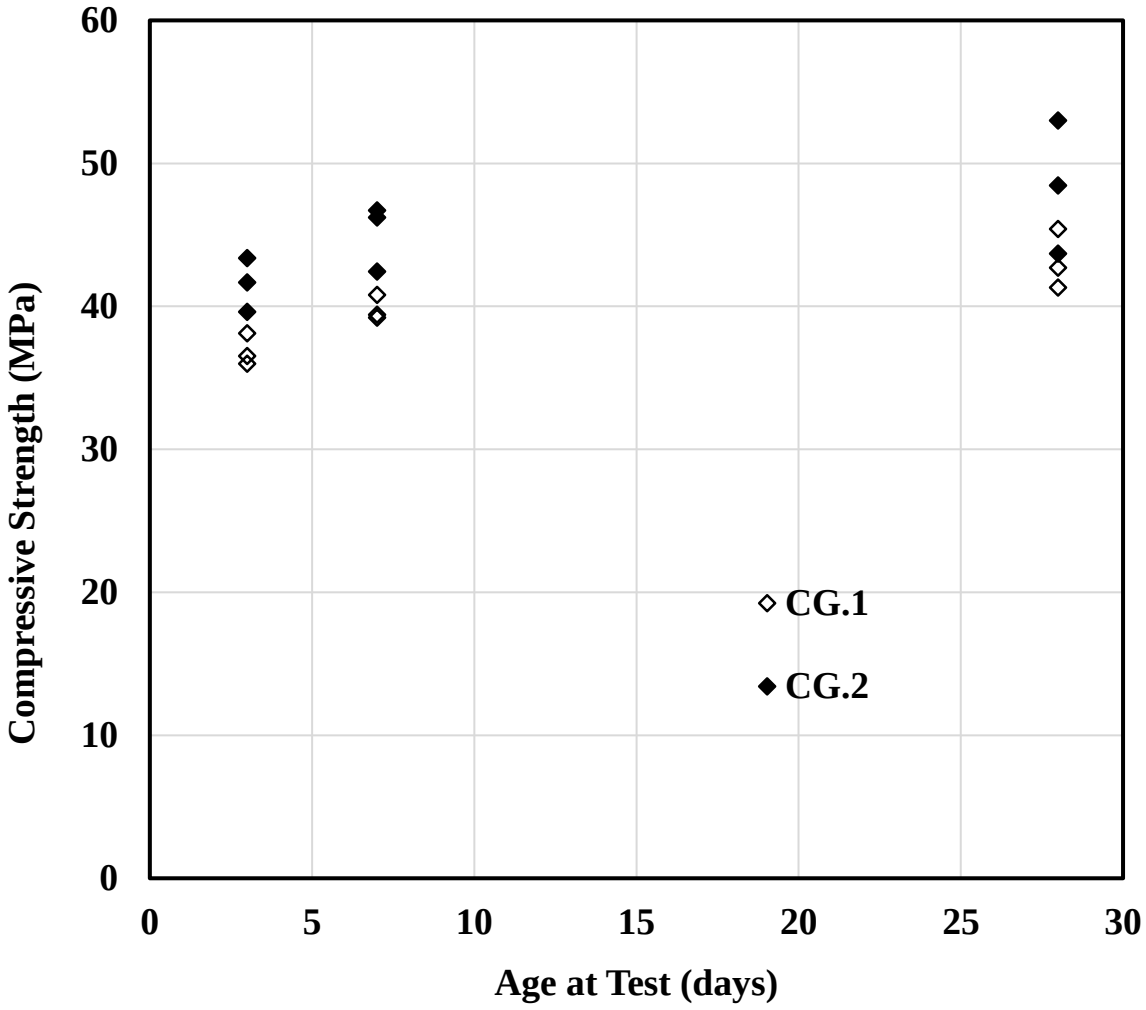

Figure 3.6 - Compressive strength results of Specimens CG.1 and CG.2.

Table 3.4 - Compressive strength results of Specimens B10.1 and B10.2.

Mix ID	Age at Test (days)	Compressive Strength (MPa)			Average Compressive Strength (MPa)
B10.1	3	32.7	32.4	33.7	32.9
	7	45.0	40.4	38.4	41.3
	28	47.7	46.6	49.6	48.0
B10.2	3	31.2	32.6	31.4	31.8
	7	36.2	36.7	24.4	32.4
	28	42.2	48.0	46.3	45.5

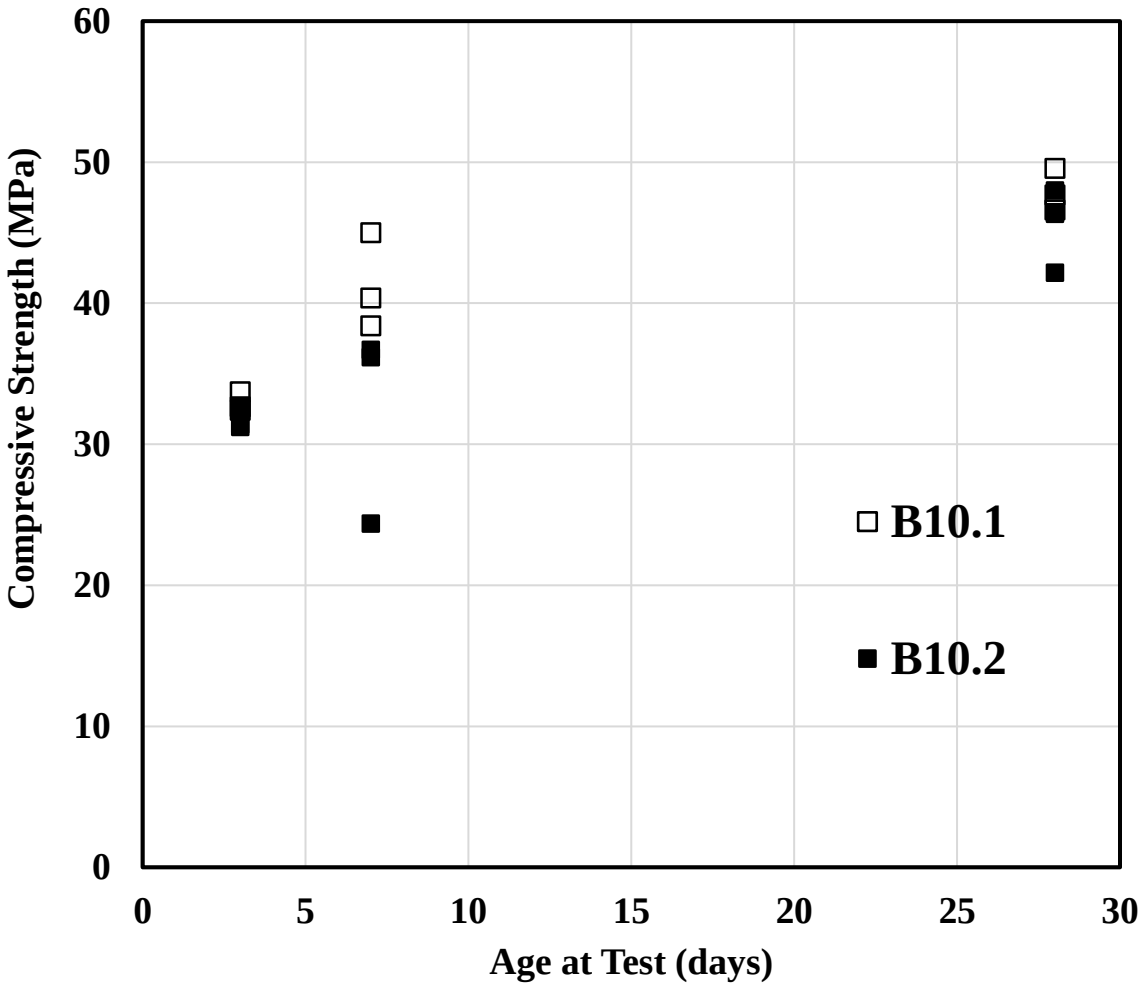

Figure 3.7 - Compressive strength results of Specimens B10.1 and B10.2.

Table 3.5 - Compressive strength results of Specimens B20.1 and B20.2.

Mix ID	Age at Test (days)	Compressive Strength (MPa)			Average Compressive Strength (MPa)
B20.1	3	38.7	36.2	33.3	36.1
	7	40.9	40.3	39.6	41.1
	28	44.9	44.4	39.6	45.9
B20.2	3	37.9	39.6	36.1	37.0
	7	35.0	47.4	43.6	41.1
	28	40.0	49.2	57.2	45.9

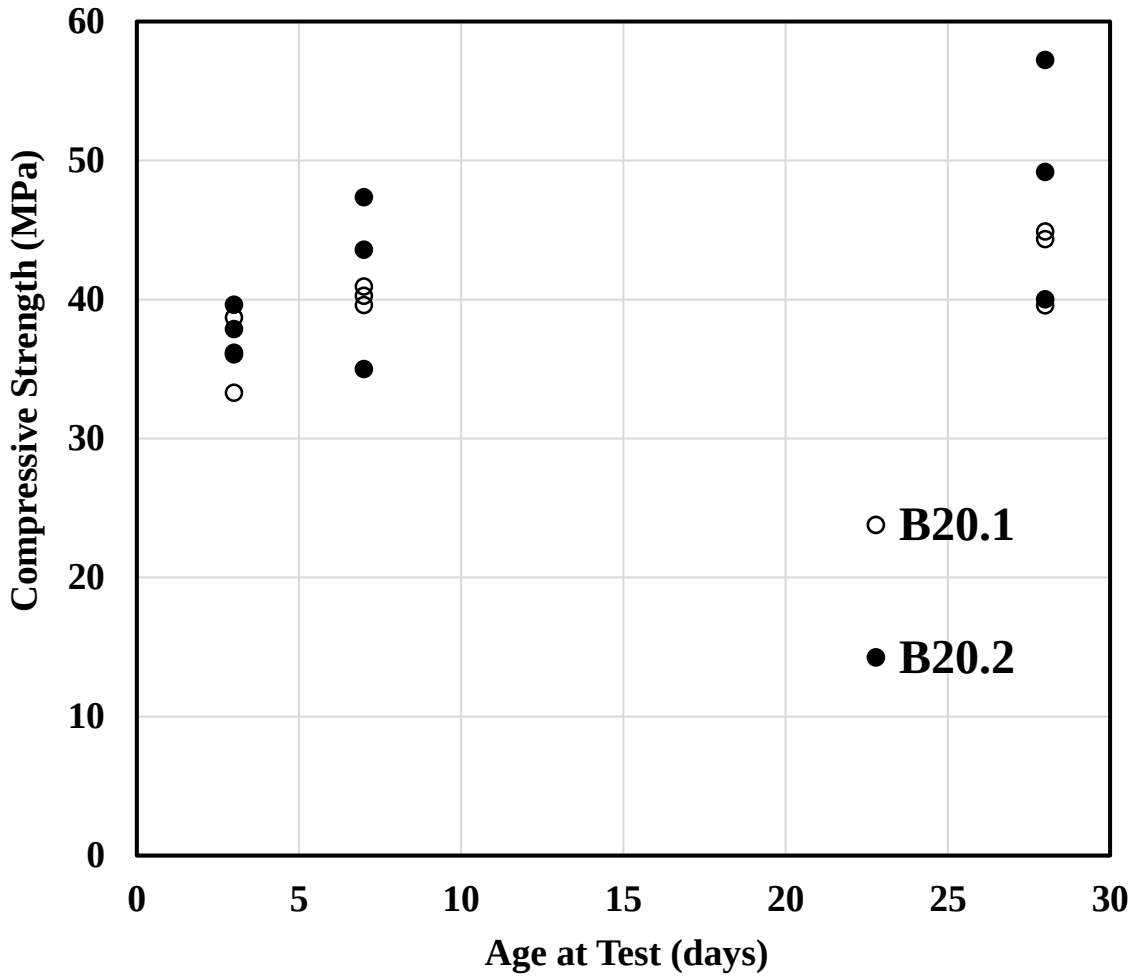

Figure 3.8 - Compressive strength results of Specimens B20.1 and B20.2.

Table 3.6 - Compressive strength results of Specimens F10.1 and F10.2.

Mix ID	Age at Test (days)	Compressive Strength (MPa)			Average Compressive Strength (MPa)
F10.1	3	34.5	38.8	40.2	38.1
	7	30.9	40.1	41.8	39.9
	28	49.5	55.0	43.4	49.6
F10.2	3	40.5	33.8	40.9	38.1
	7	46.8	43.1	36.3	39.9
	28	53.8	49.0	47.1	49.6

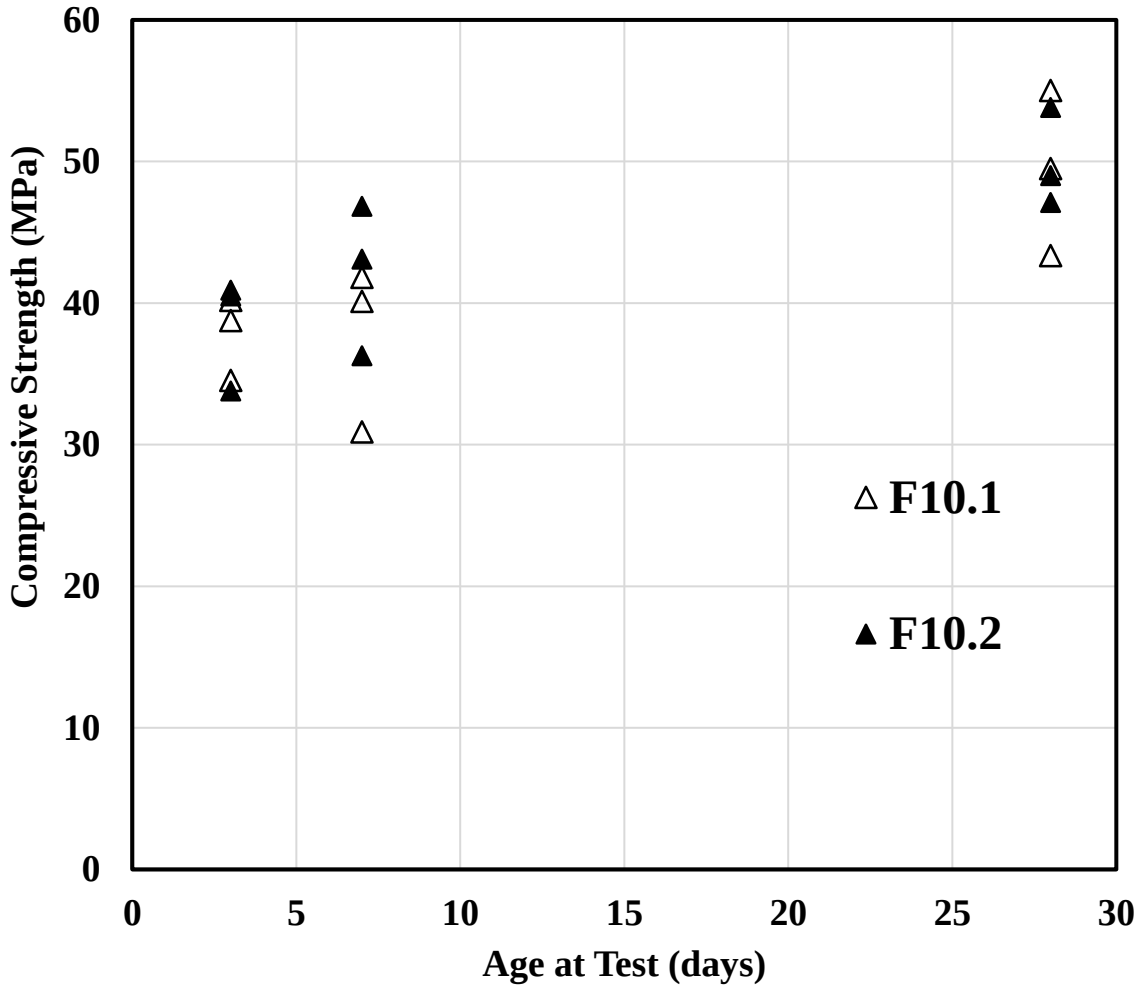

Figure 3.9 - Compressive strength results of Specimens F10.1 and F10.2.

Table 3.7 - Compressive strength results of Specimens F20.1 and F20.2.

Mix ID	Age at Test (days)	Compressive Strength (MPa)			Average Compressive Strength (MPa)
F20.1	3	37.6	41.8	39.2	36.5
	7	48.1	44.3	38.4	42.8
	28	50.1	47.6	42.9	47.4
F20.2	3	30.4	34.3	35.5	36.5
	7	40.1	44.0	41.8	42.8
	28	49.8	45.6	48.5	47.4

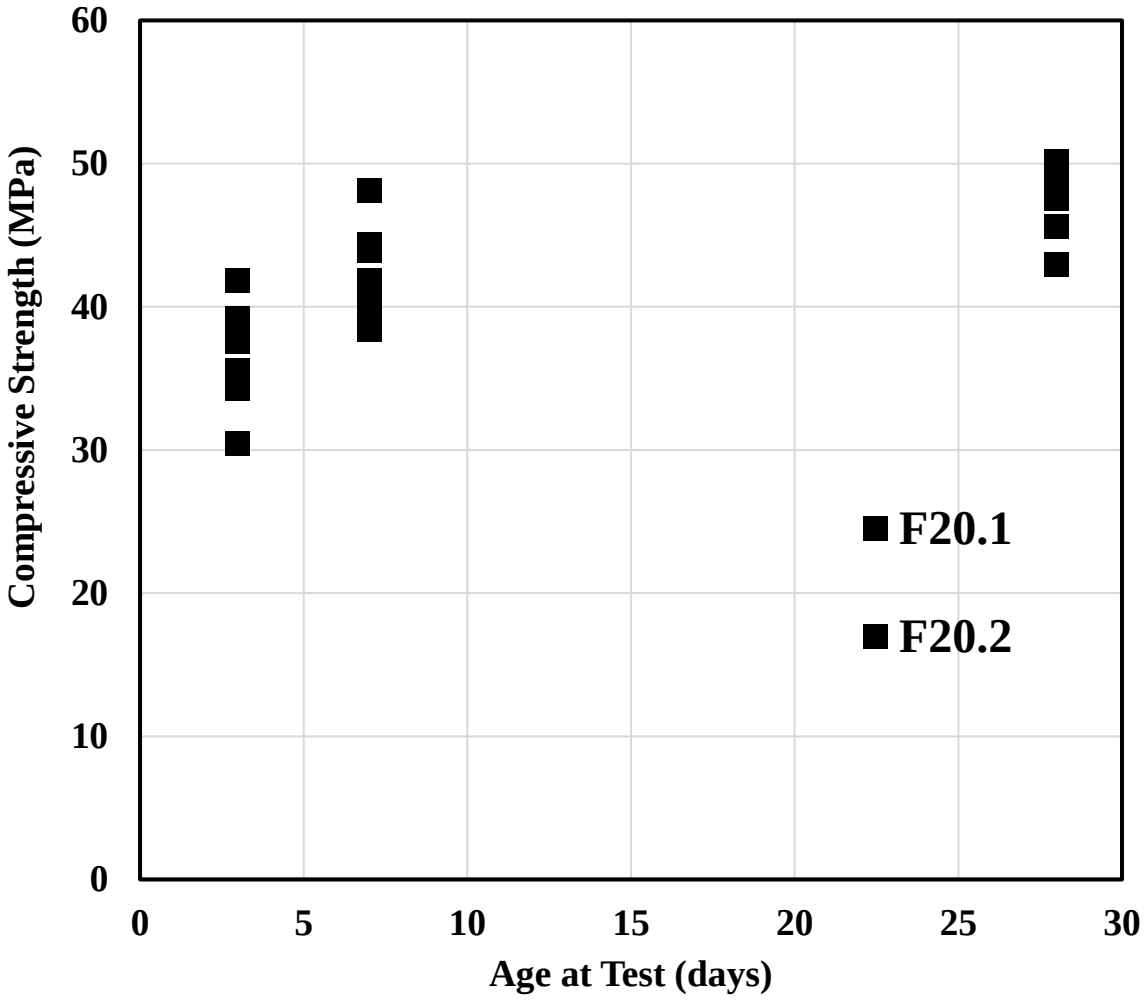

Figure 3.10 - Compressive strength results of Specimens F20.1 and F20.2.

Table 3.8 - Compressive strength results of Specimens OS.1 and OS.2.

Mix ID	Age at Test (days)	Compressive Strength (MPa)			Average Compressive Strength (MPa)
OS.1	3	38.2	39.7	37.4	39.0
	7	44.0	40.6	45.9	40.3
	28	52.1	52.7	49.9	49.8
OS.2	3	41.6	38.2	39.0	39.0
	7	29.1	42.3	39.6	40.3
	28	44.4	47.6	51.7	49.8

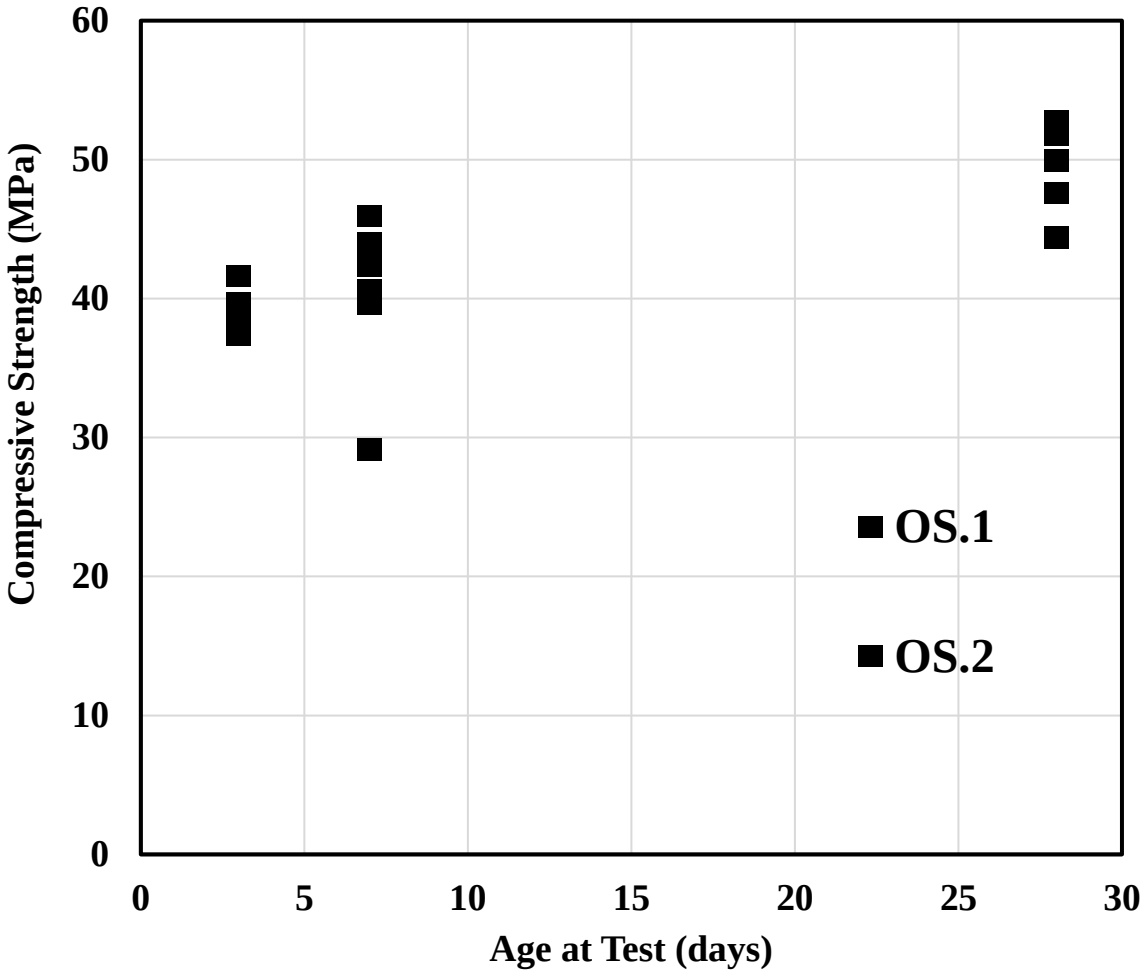

Figure 3.11 - Compressive strength results of Specimens OS.1 and OS.2.

Table 3.9 - Average compressive strength results of all specimens.

Mix ID	Average Compressive Strength (MPa)			Symbol
	At 3 days	At 7 days	At 28 days	
CG (CG.1 + CG.2)	39.2	42.5	45.8	◇
B10 (B10.1+B10.2)	32.3	36.8	46.7	□
B20 (B20.1+B20.2)	37.0	41.1	45.9	○
F10 (F10.1+F10.2)	38.1	39.9	49.6	△
F20 (F20.1+F20.2)	36.5	42.8	47.4	▽
OS (OS.1+OS.2)	39.0	40.3	49.8	⬡

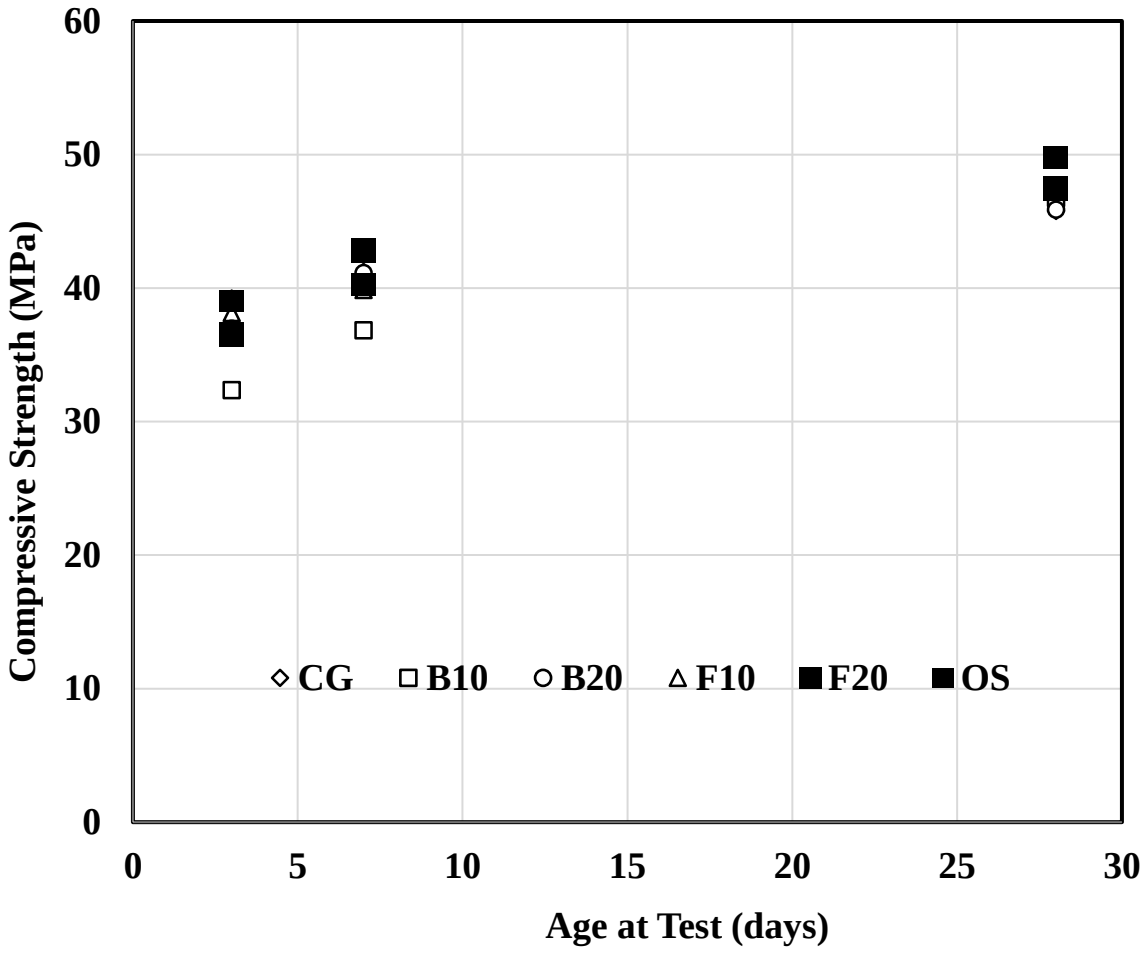

Figure 3.12 - Average compressive strength results of all specimens.

Table 3.10 - Average compressive strengths of all specimens normalized by the required results.

Mix ID	Average Compressive Strength			
	At 7 days		At 28 days	
	Computed (MPa)	Normalized by Required Result*	Computed (MPa)	Normalized by Required Result**
CG	42.5	2.02	45.8	1.31
B10	36.8	1.75	46.7	1.34
B20	41.1	1.96	45.9	1.31
F10	39.9	1.90	49.6	1.42
F20	42.8	2.04	47.4	1.35
OS	40.3	1.92	49.8	1.42

* PTI M55 requires that compression strength of grout must be at least 21 MPa at age 7 days.
** PTI M55 requires that compression strength of grout must be at least 35 MPa at age 28 days.

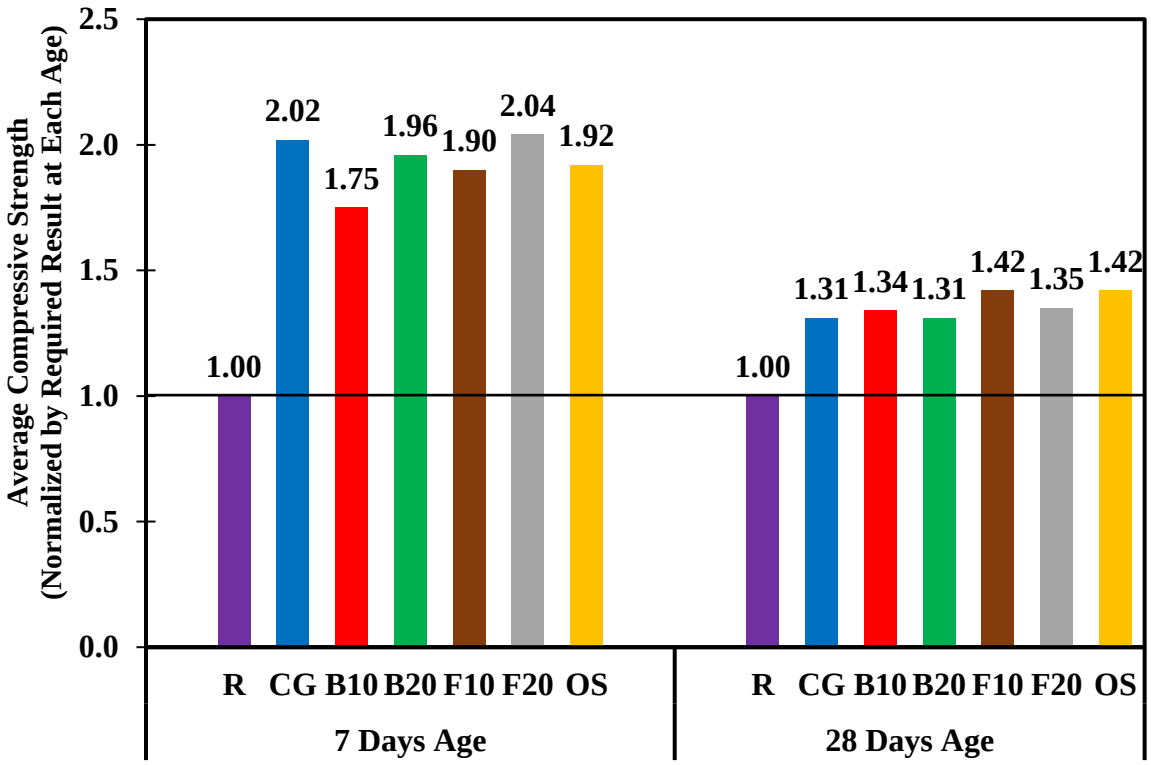

Figure 3.13 - Normalized average compressive strengths of all specimens compared to the required results (R).

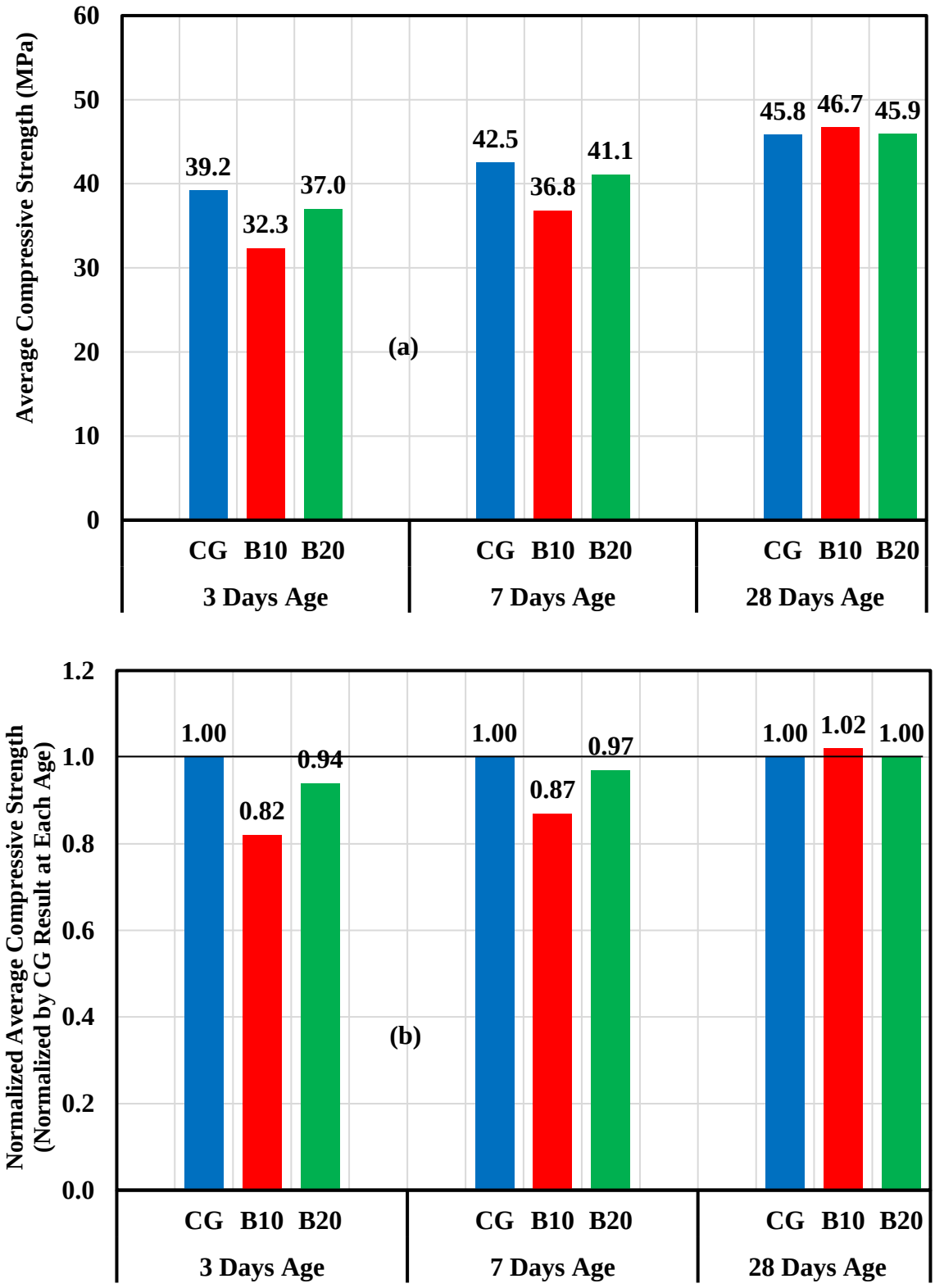

Figure 3.14 - (a) Average and (b) normalized compressive strengths of grouts containing barium carbonate compared to conventional grout.

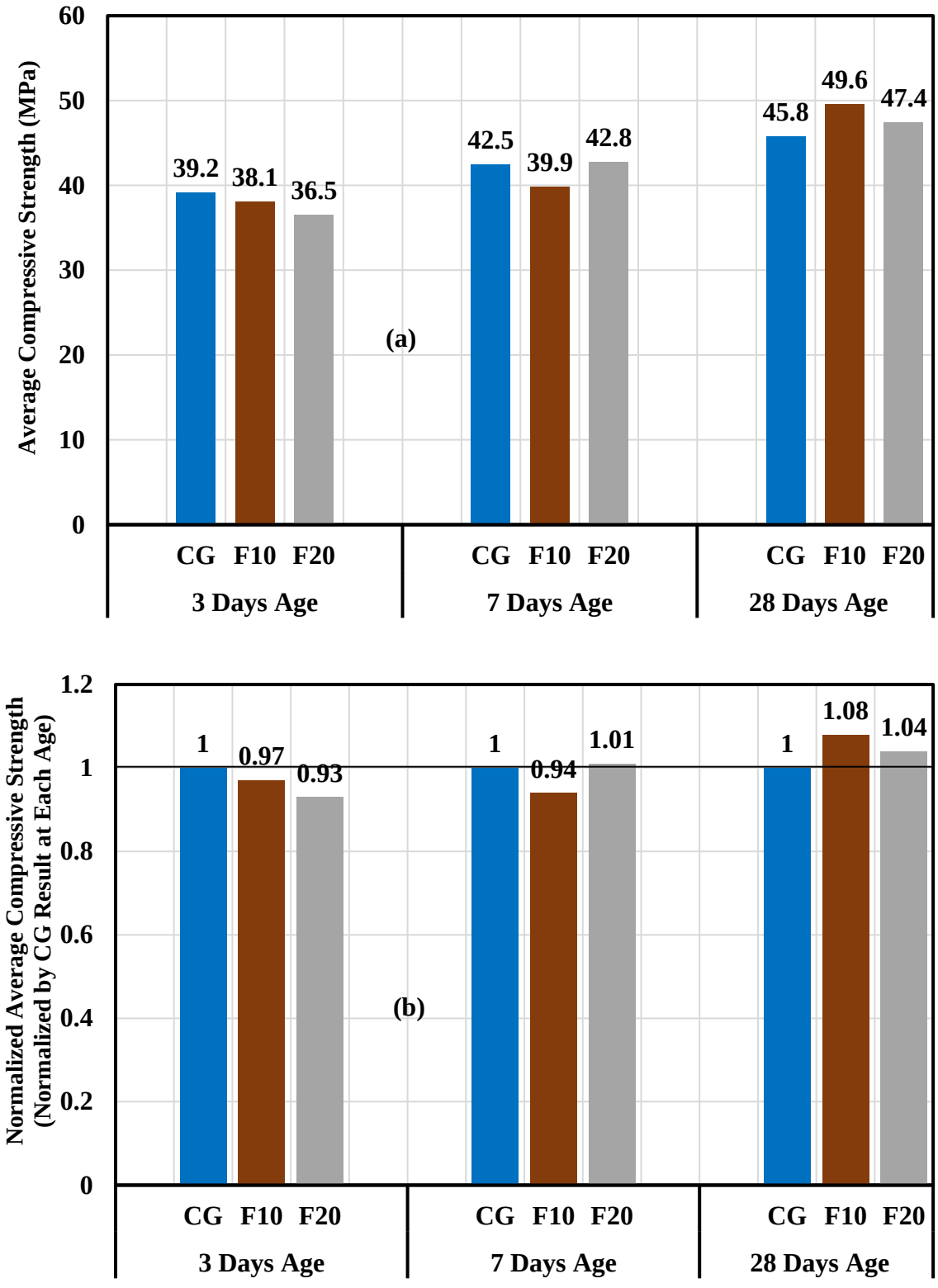

Figure 3.15 - (a) Average and (b) normalized compressive strengths of grouts containing iron oxide compared to conventional grout.

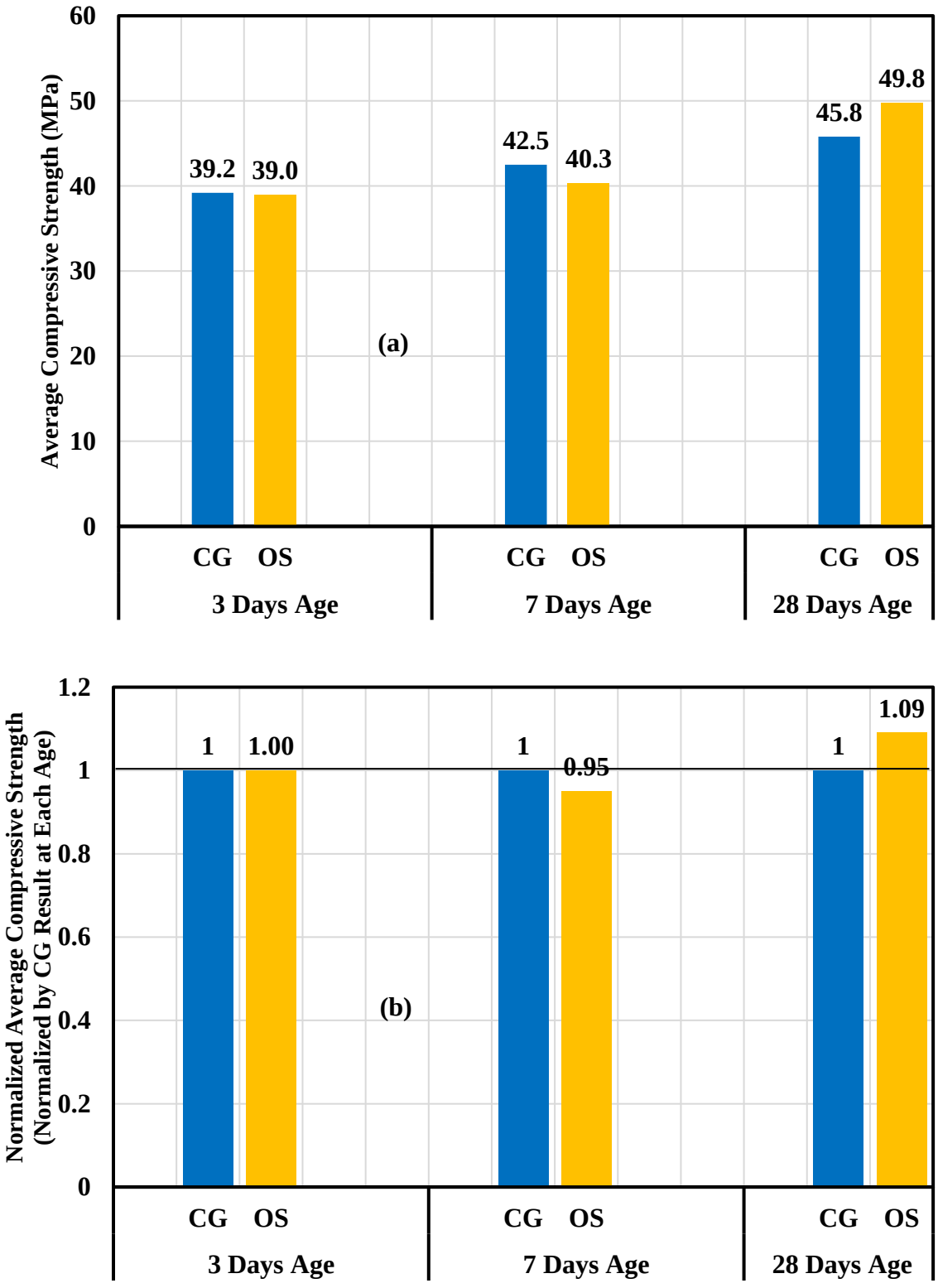

Figure 3.16 - (a) Average and (b) normalized compressive strengths of grouts containing Ottawa Sand compared to conventional grout.

CHAPTER 4

WICK-INDUCED BLEED TESTS

4.1 INTRODUCTION

This chapter presents the bleed tests. A description of the experimental program is provided in Section 4.2. This includes a description of the test matrix, specimen mixture proportions, as well as details of specimen preparation and testing. After that, Section 4.3 presents the experimental results of all specimens. Next, a discussion of these results is presented in Section 4.4. Finally, the conclusions of this chapter are presented in Section 4.5.

Previous work by Keller and Pessiki (2016) demonstrated that barium carbonate is more efficient as a photon attenuating material as compared to iron. Because both barium carbonate and iron grouts satisfy strength requirements of PTI M55, but barium carbonate is more effective as a PAI, only barium carbonate is investigated in the bleed tests described in this chapter.

4.2 DESCRIPTION OF EXPERIMENTAL PROGRAM

4.2.1 Test Matrix

The test matrix for bleed tests is shown in Table 4.1. As shown in the table, two groups of specimens were tested (CG and B20). CG refers to the specimens that were conventional grout, made with only Type I Portland cement and water. B20 refers to specimens made with 20% by weight barium carbonate ($BaCO_3$).

A total of 4 different mixtures were batched, denoted with the 4 Specimen ID notations given in Table 4.1. Each replicate batch is given a numeric identifier. For example, the two batches of conventional grout are identified as CG.1 and CG.2.

4.2.2 Mixture Proportions

Mixture proportions of all specimens are shown in Table 4.2. As shown in the table, 4 different grout batches were tested. Each batch was intended to fill about 900 mm length of about 79 mm internal diameter tube. About 6000 cm^3 of grout was mixed for each of Specimens CG.1 and CG.2.

As noted in Section 3.5, the addition of barium carbonate to the grout mix caused a noticeable thickening of the grout as compared to the conventional grout consisting of only cement and water. It was expected that the barium carbonate grout would result in more wasted material as it adhered in a thicker coating to the mixer, tools, and grout pump. Therefore, a slightly large volume (7000 cm^3) was batched.

To be consistent with the compression tests described in Section 3, the water/cement ratio for all batches was fixed at 0.45.

4.2.3 Specimen Preparation

All mixing tools and dry ingredients, as well as mixing water were prepared and set in the laboratory one day prior to testing. On the testing day, all ingredients were mixed in a 19-liter bucket using a hand-held drill with a paddle tool as follows: the dry ingredients were mixed manually first to make certain they were well blended. Then, the water was added into a clean 19-liter bucket. After that, the dry ingredients were added gradually to the bucket containing the water over a time span of 1 and 2 minutes for Specimens CG and

B20, respectively. It is noted that dry material was added more slowly to the B20 mixture because of the thickening that was observed. After 2 minutes from the start of mixing, the mixing was paused for 1 minute to scrape down into the bucket any material stuck on its side. Finally, the mixing was resumed for 1 additional minute.

The grout was then poured from the mixing bucket into the reservoir of a grout pump. Figure 4.1 shows the grout pump that was used in bleed tests.

Afterward, the grout was injected at top of tube up to roughly 900 mm of the 1000-mm high tube and its initial level was recorded. Next, a 1170 mm length of seven-wire 15.24 mm diameter strand, which was brushed and degreased with acetone, was inserted into the tube. In order to reduce evaporation, the top of the tube was covered using masking tape.

The initial height of the grout column in the tube ranged between 889 mm and 914 mm for the four specimens

4.2.4 Measurements

After injecting the grout, the levels of both the grout and water were recorded periodically, using a ruler attached to the tube, for 15 minute increments and up to 120 minutes after starting the grout injection. Figure 4.2 shows the tube (a) before and (b) after being filled with grout. Finally, after 120 minutes from the start of the grout injection, the bleed water was decanted using a plastic pipette into a glass graduated cylinder, and the volume of the decanted water was recorded. Figure 4.3 shows the water level and the grout level at the top of Specimens CG.2 and B20.2 at the end of the test.

4.3 EXPERIMENTAL RESULTS

The experimental results are presented in this section. Section 4.3.1 presents the results for the conventional grout specimens. Results for the grouts made with barium carbonate are presented in Section 4.3.2. All bleed results are read and recorded to nearest 1 mm.

4.3.1 Grout CG (CG.1 and CG.2)

Two replicate batches of conventional grout, (CG.1 and CG.2), which had ordinary Type I cement and water, were made and tested for bleeding up to 2 hours. The two batches were made and tested on two different days. Levels of grout and water at 15 minute increments for Specimens CG.1 and CG.2 are presented in Table 4.3 and Table 4.4, respectively. Furthermore, the differences in grout level and water level with reference to their initial levels for both Specimens CG.1 and CG.2 are shown in Figure 4.4 and Figure 4.5, respectively. Negative numbers on the y-axis indicate that the level is under the first reading height, taken after injection of grout.

The volume of the decanted water at the end of the two hours was 112.2 cm^3 and 135 cm^3 for Specimens CG.1 and CG.2, respectively.

4.3.2 Grout B20 (B20.1 and B20.2)

Two batches of B20, (B20.1 and B20.2), which had ordinary Type I cement, water, and barium carbonate, were made and tested for bleeding up to 2 hours. The two batches were made and tested on two different days. Levels of grout and water at 15 minute increments for Specimens B20.1 and B20.2 are presented in Table 4.5 and Table 4.6, respectively. Furthermore, the differences in grout level and water level with reference to

their initial levels for both Specimens B20.1 and B20.2 are shown in Figure 4.6 and Figure 4.7, respectively.

The volume of the decanted water at the end of the two hours was 16 cm^3 and 7.45 cm^3 for Specimens B20.1 and B20.2, respectively.

4.4 DISCUSSION OF WICK-INDUCED BLEED TEST RESULTS

Results obtained from performing the bleed test on the four specimens are discussed in this section. For each specimen, three values are computed from the measured values reported in the tables: expansion of grout; grout bleeding; and combined expansion of grout and bleed water. According to ASTM C940, three different equations shall be used to determine these values.

The expansion of the grout during each prescribed interval is calculated by the following equation:

$$\text{Expansion of grout, \%} = \frac{V_g - V_1}{V_1} \times 100 \tag{4.1}$$

The percent bleeding of the grout during each prescribed interval is computed by the following equation:

$$\text{Bleeding, \%} = \frac{V_2 - V_g}{V_1} \times 100 \tag{4.2}$$

Equation 4.2 is the one to compare to PTI M55 value of 0.0%.

The combined percent expansion of both the grout and the bleed water is calculated using the following equation:

$$\text{Combined expansion}, \% = \frac{V_2 - V_1}{V_1} \times 100 \quad (4.3)$$

Where:

V_1 = Volume of specimen at the beginning of test, cm^3,

V_2 = Volume of specimen at prescribed intervals, measured at the upper surface of the water level, cm^3, and

V_g = Volume of the grout portion of the specimen at prescribed intervals, at the upper surface of the grout level, cm^3.

At the end of the test, the final bleeding (%) of grout is calculated by dividing the volume of bleed water, decanted from the top of the specimen into the glass graduated cylinder, to the volume of the specimen at the beginning of the test. The following equation is used to calculate the final bleeding:

$$\text{Final bleeding}, \% = \frac{V_w}{V_1} \times 100 \quad (4.4)$$

Where:

V_w = Volume of decanted bleed water, cm^3.

4.4.1 Effect of Barium Carbonate on Grout Expansion

Results obtained from Equations 4.1 and 4.3 for both Specimens CG.1 and CG.2 are presented in Table 4.7 and Table 4.8, respectively. It is noted that the volume of the grout for both specimens reduced with time, the minus sign indicates that the grout level is lower than its level at the beginning of the test. Moreover, it can be seen that the combined expansion of grout plus bleed water for Specimen CG.1 became zero within 60 minutes of starting the test; indicating that level of the Specimen is equal to its level at the beginning of the test.

On the other hand, Table 4.9 and Table 4.10 show results obtained from Equations 4.1 and 4.3 for Specimens B20.1 and B20.2, respectively. It can be seen that levels of grout and water of Specimen B20.1 became constant after 30 minutes of injecting the grout and fixed at all intervals for Specimen B20.2. Because the water level at each prescribed interval was constant and was equal to the first reading of specimen height, the combined expansion of Specimen B20.1 is zero at each interval.

4.4.2 Effect of Barium Carbonate on Grout Bleeding

The percentages of bleed water of all four specimens are tabulated in Table 4.11 and plotted in Figure 4.8. Results at each interval were computed using Equation 4.2. For the conventional grouts, the percentages of bleed water at the end of the two hours were 2.64% and 3.25% for Specimens CG.1 and CG.2, respectively, while they were 0.43% and 0.21% for Specimens B20.1 and B20.2, respectively. Compared to conventional grout, it can be seen that using barium carbonate improved the ability of grout to resist bleeding.

For instance, the percentage of the average bleed water of grout made with barium carbonate at the end of the test is:

$$\frac{0.43 + 0.21}{2} = 0.32$$

While for the conventional grout it is:

$$\frac{2.64 + 3.25}{2} = 2.95$$

Therefore, grouts made with barium carbonate exhibited less bleeding than the conventional grout by:

$$\frac{2.95 - 0.32}{2.95} * 100 = 89\ \%$$

Changes in grout bleeding between each consecutive recorded interval during the two hours test are tabulated in Table 4.12 and plotted in Figure 4.9. It is noted from the results that the change in bleed water of Specimens B20.1 and B20.2 became zero after 45 and 30 minutes, respectively, of starting the readings. This indicates that the percentages of bleed water of each specimen, with respect to each initial volume, were constant after these specified times. On the other hand, Specimens CG.1 and CG.2 needed 90 and 60 minutes, respectively, to exhibit a stabilized bleed water.

Using Equation 4.4, the percentages of the final bleed water of all specimens were slightly different from results computed using Equation 4.2. The percentages of the final bleed water, using Equation 4.4, were 2.49% and 2.96% for Specimens CG.1 and CG.2, respectively and 0.35% and 0.16% for Specimens B20.1 and B20.2, respectively. The differences in results between the two equations, (4.2 and 4.4), might be due to the uneven

surface at the top of the grout level of each specimen which can be seen clearly in Figure 4.3.

4.5 CONCLUSIONS FROM WICK-INDUCED BLEED TESTS

The following conclusions are drawn from bleed tests:

1. Grout made with barium carbonate exhibits less bleeding that conventional grout made with only cement and water.
2. The conventional grout, which made with cement and water, exhibited a large volume of bleed water at the end of the test; moreover, the bleed water was observed clearly at the beginning of the test.
3. Although its contribution to reduce bleeding was observed clearly during the experiment, grouts made with only cement, water, and barium carbonate might not be attaining the requirement of the PTI, which is 0.0% at three hours.

Table 4.1 - Test matrix for wick-induced bleed tests.

Group	Mix ID	Comments
CG	CG.1	Type I Portland cement + water
	CG.2	
B20	B20.1	Type I Portland cement + 20% barium carbonate + water
	B20.2	

Table 4.2 - Mixture proportions for the wick-induced bleed test.

Mix ID	Mixture Proportions (grams)			Comments
	Cement	Water	$BaCO_3$	
CG.1	7818	3518	0	Conventional grout
CG.2	7818	3518	0	
B20.1	8599	3870	1720	20% barium carbonate
B20.2	8599	3870	1720	

Figure 4.1 - Photograph of grout pump used to pour grout into test tube.

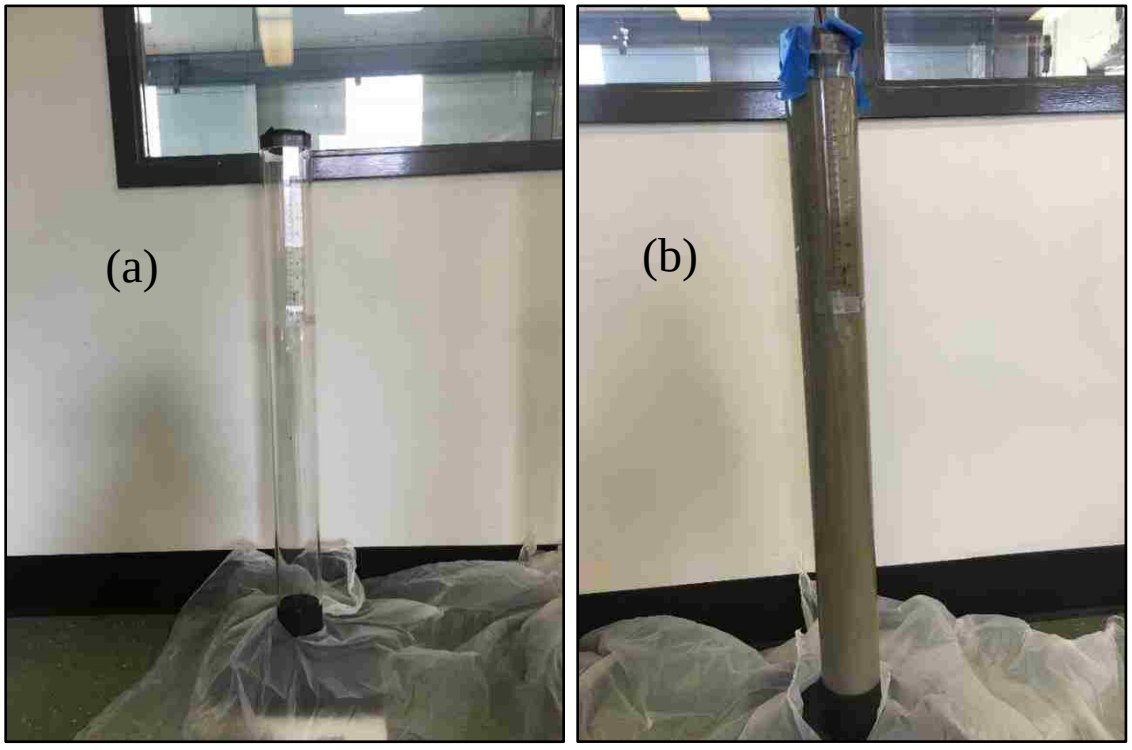

Figure 4.2 - The tube (a) before and (b) after injection of grout.

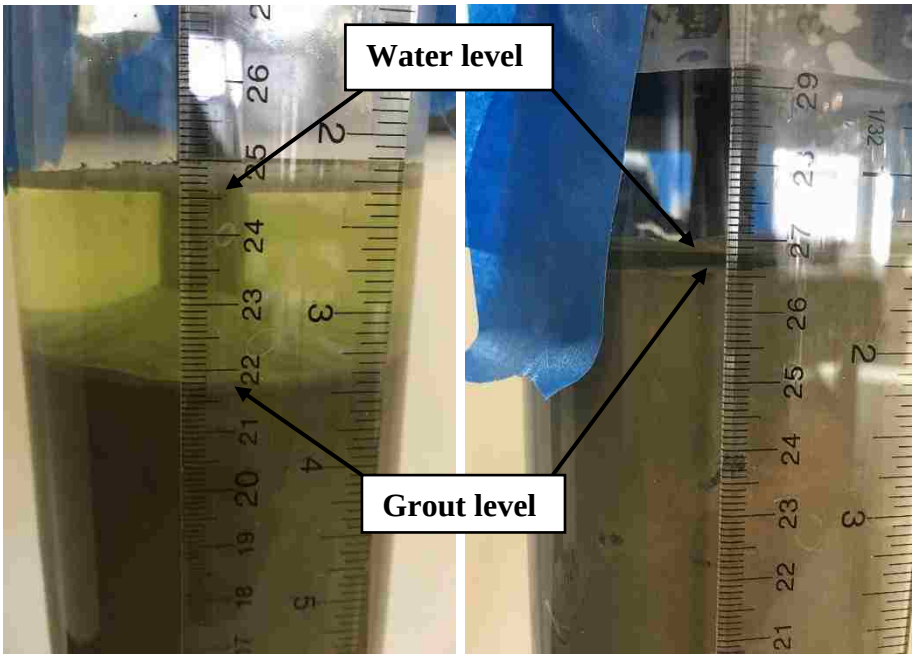

Figure 4.3 - Top of Specimens CG.2 (left) and B20.2 (right) two hours after being injected.

Table 4.3 - Height of grout and water of Specimen CG.1.

Elapsed Time (minutes)	Height of Grout (mm)	Height of Water (mm)
0 (before strand)	889	889
0 (after strand)	909	909
15	897	913
30	888	912
45	886	912
60	886	909
75	885	909
90	885	909
105	885	909
120	885	909

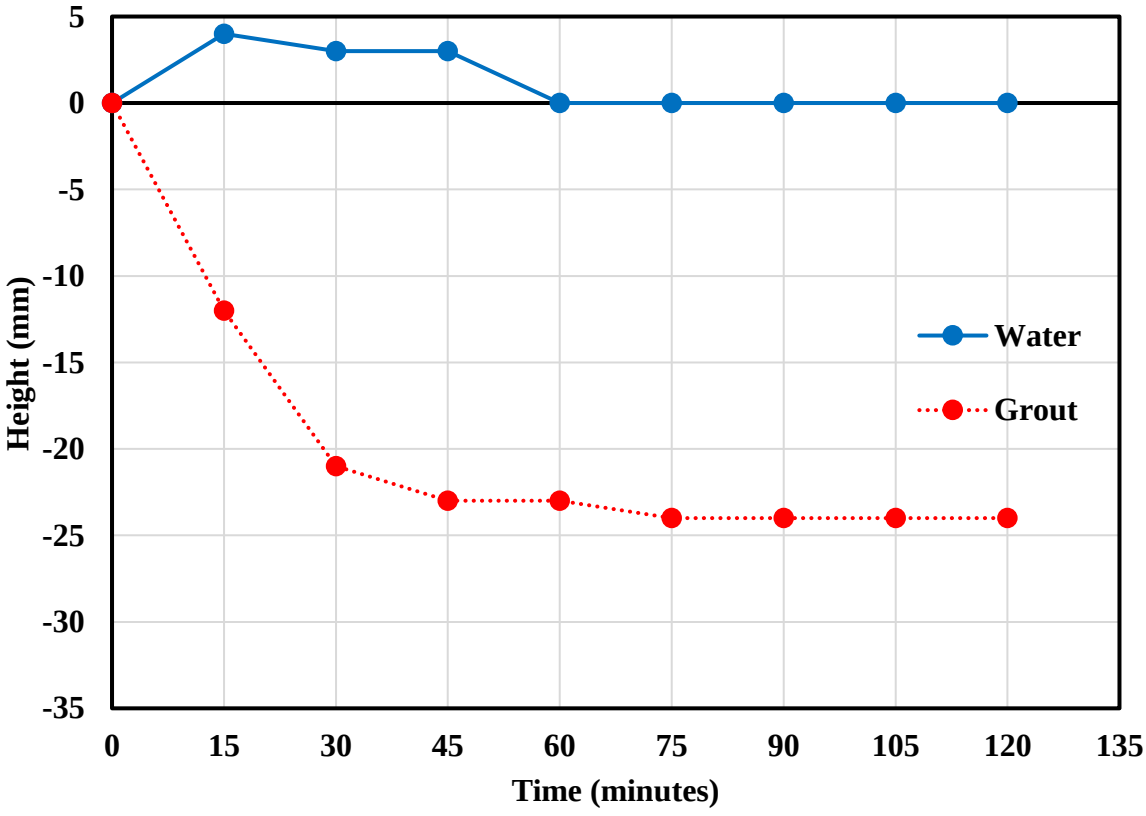

Figure 4.4 - Changes in heights of grout and water of Specimen CG.1 with reference to their initial heights.

Table 4.4 - Height of grout and water of Specimen CG.2.

Elapsed Time (minutes)	Height of Grout (mm)	Height of Water (mm)
0 (before strand)	896	896
0 (after strand)	923	923
15	903	921
30	893	921
45	890	920
60	890	920
75	890	920
90	890	920
105	890	920
120	890	920

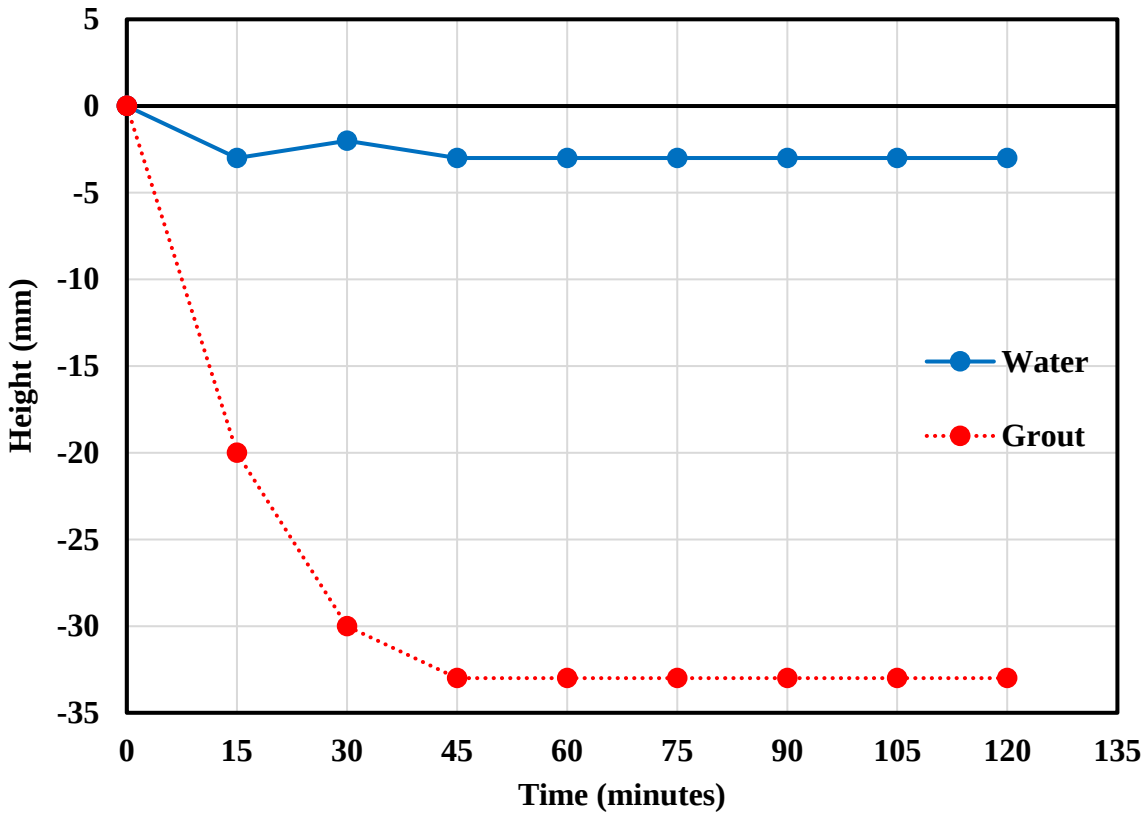

Figure 4.5 - Changes in heights of grout and water of Specimen CG.2 with reference to their initial heights.

Table 4.5 - Height of grout and water of Specimen B20.1.

Elapsed Time (minutes)	Height of Grout (mm)	Height of Water (mm)
0 (before strand)	901	901
0 (after strand)	926	926
15	923	926
30	922	926
45	922	926
60	922	926
75	922	926
90	922	926
105	922	926
120	922	926

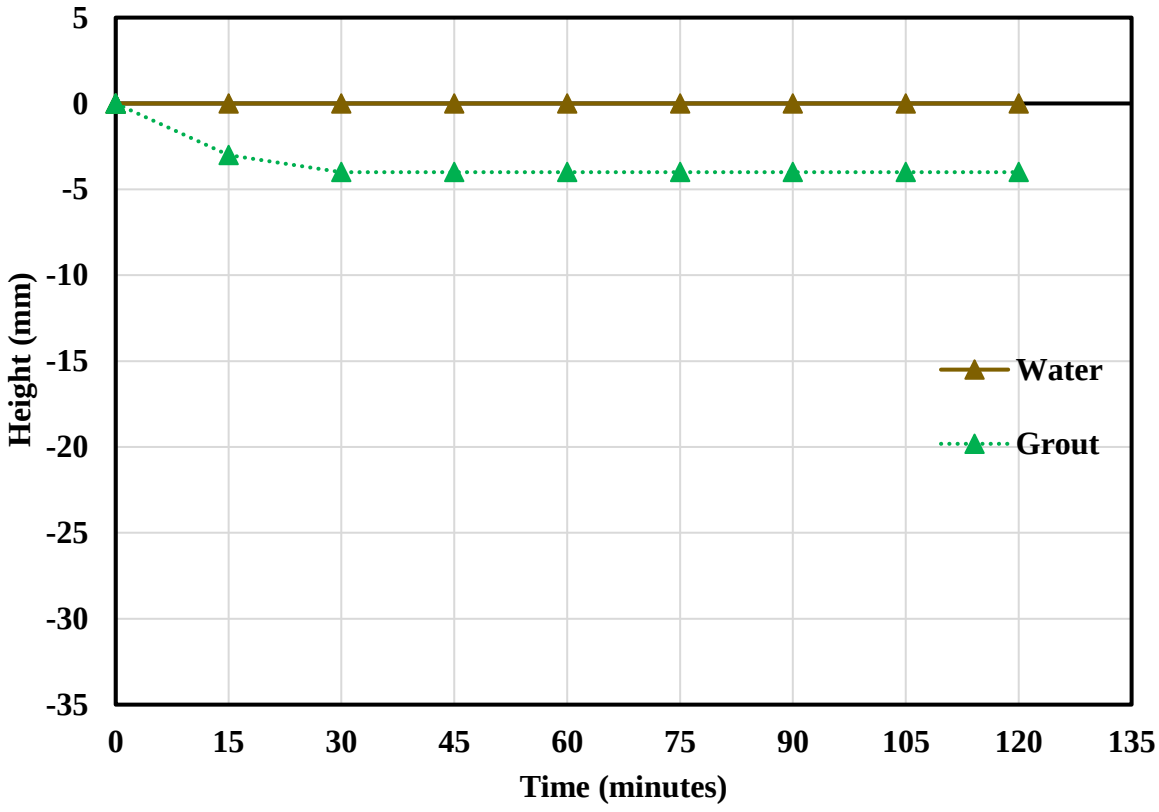

Figure 4.6 - Changes in heights of grout and water of Specimen B20.1 with reference to their initial heights.

Table 4.6 - Height of grout and water of Specimen B20.2.

Elapsed Time (minutes)	Height of Grout (mm)	Height of Water (mm)
0 (before strand)	914	914
0 (after strand)	943	943
15	939	941
30	939	941
45	939	941
60	939	941
75	939	941
90	939	941
105	939	941
120	939	941

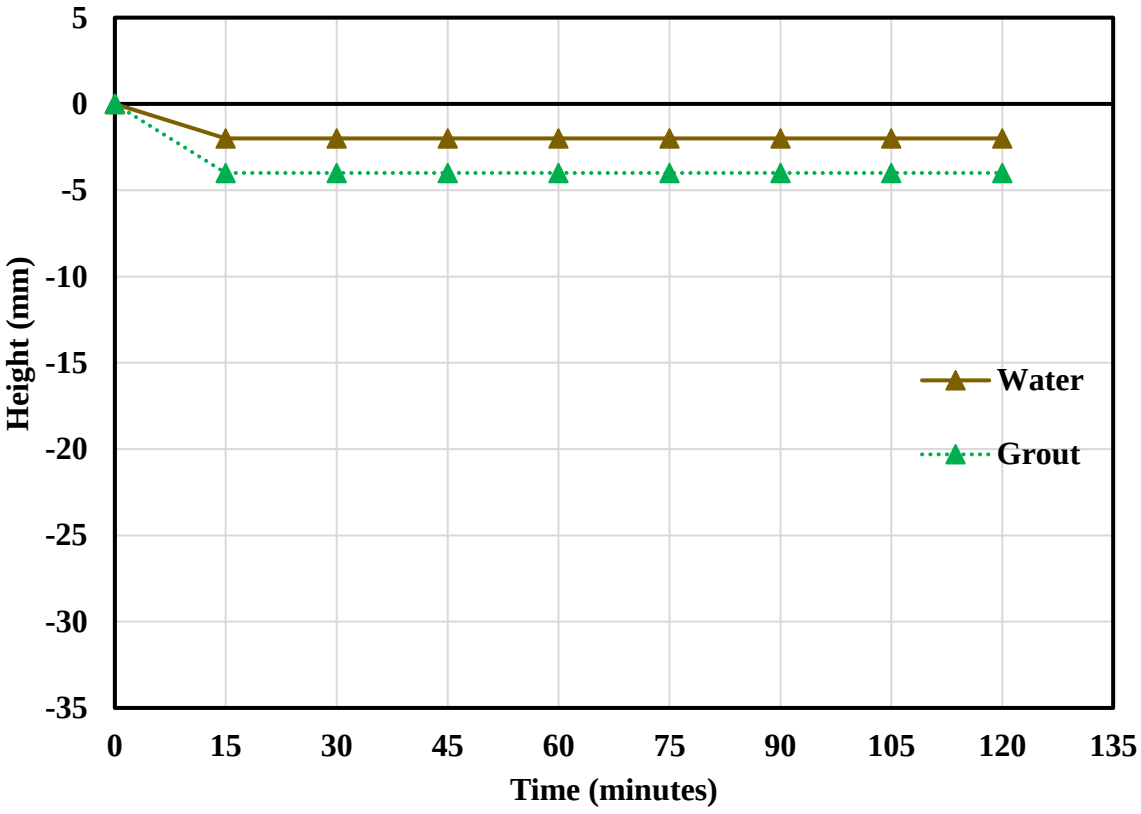

Figure 4.7 - Changes in heights of grout and water of Specimen B20.2 with reference to their initial heights.

Table 4.7 - Expansion of Specimen CG.1.

Elapsed Time (minutes)	Expansion of Grout, %	Combined Expansion, %
15	**-1.32**	**0.44**
30	**-2.31**	**0.33**
45	**-2.53**	**0.33**
60	**-2.53**	**0.00**
75	**-2.64**	**0.00**
90	**-2.64**	**0.00**
105	**-2.64**	**0.00**
120	**-2.64**	**0.00**

Table 4.8 - Expansion of Specimen CG.2.

Elapsed Time (minutes)	Expansion of Grout, %	Combined Expansion, %
15	**-2.17**	**-0.33**
30	**-3.25**	**-0.22**
45	**-3.58**	**-0.33**
60	**-3.58**	**-0.33**
75	**-3.58**	**-0.33**
90	**-3.58**	**-0.33**
105	**-3.58**	**-0.33**
120	**-3.58**	**-0.33**

Table 4.9 - Expansion of Specimen B20.1.

Elapsed Time (minutes)	Expansion of Grout, %	Combined Expansion, %
15	**-0.32**	**0.00**
30	**-0.43**	**0.00**
45	**-0.43**	**0.00**
60	**-0.43**	**0.00**
75	**-0.43**	**0.00**
90	**-0.43**	**0.00**
105	**-0.43**	**0.00**
120	**-0.43**	**0.00**

Table 4.10 - Expansion of Specimen B20.2.

Elapsed Time (minutes)	Expansion of Grout, %	Combined Expansion, %
15	**-0.42**	**-0.21**
30	**-0.42**	**-0.21**
45	**-0.42**	**-0.21**
60	**-0.42**	**-0.21**
75	**-0.42**	**-0.21**
90	**-0.42**	**-0.21**
105	**-0.42**	**-0.21**
120	**-0.42**	**-0.21**

Table 4.11 - Percentages of bleed water of all specimens.

Elapsed Time (minutes)	Bleeding, % $\frac{V_2 - V_g}{V_1} \times 100$			
	CG		B20	
	CG.1	CG.2	B20.1	B20.2
15	1.76	1.84	0.32	0.21
30	2.64	3.03	0.43	0.21
45	2.86	3.25	0.43	0.21
60	2.53	3.25	0.43	0.21
75	2.64	3.25	0.43	0.21
90	2.64	3.25	0.43	0.21
105	2.64	3.25	0.43	0.21
120	2.64	3.25	0.43	0.21

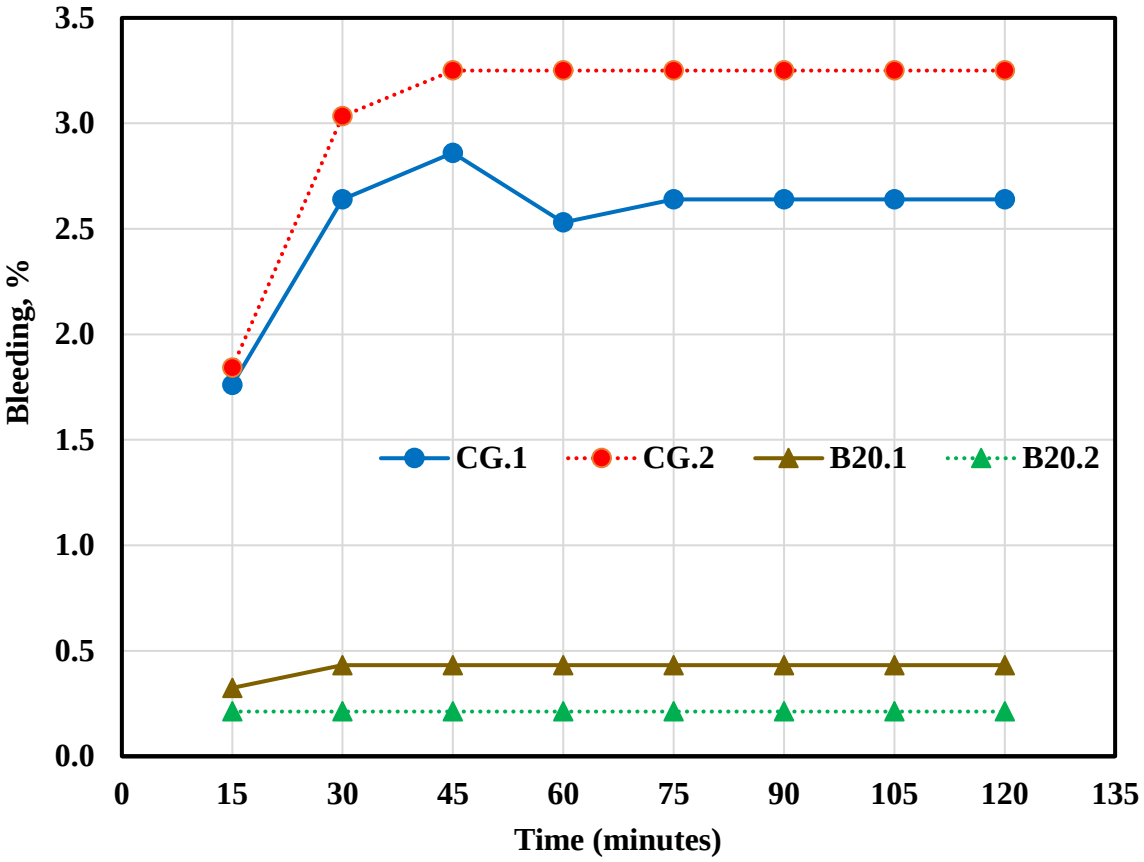

Figure 4.8 - Percentages of bleed water of all specimens.

Table 4.12 - Change in bleed water of all specimens.

Elapsed Time (minutes)	Relative Bleeding, %			
	CG		B20	
	CG.1	CG.2	B20.1	B20.2
30	0.88	1.19	0.11	0.00
45	0.22	0.22	0.00	0.00
60	-0.33	0.00	0.00	0.00
75	0.11	0.00	0.00	0.00
90	0.00	0.00	0.00	0.00
105	0.00	0.00	0.00	0.00
120	0.00	0.00	0.00	0.00

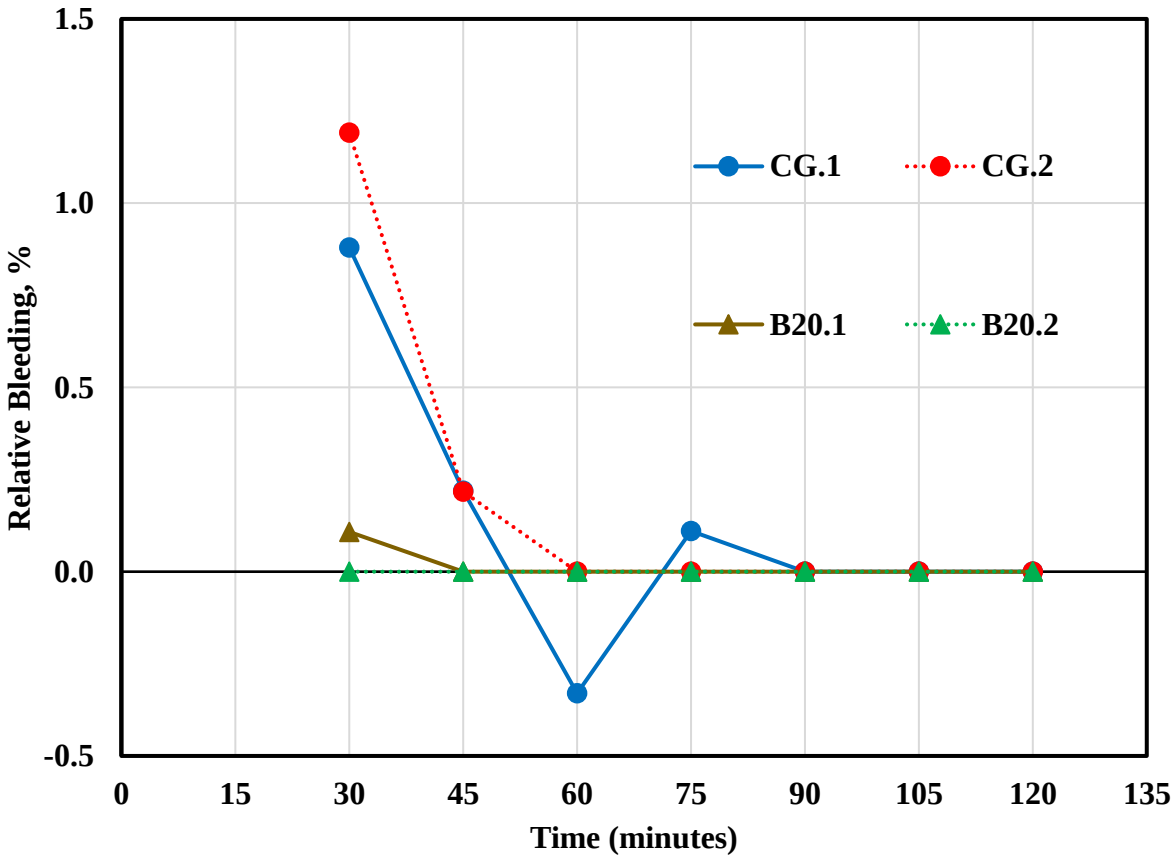

Figure 4.9 - Change in bleed water of all specimens.

CHAPTER 5

RADIOGRAPHY TESTS

5.1 INTRODUCTION

This chapter presents the radiography tests performed on the grout specimens. A description of the experimental program is provided in Section 5.2. This includes a description of the test matrix, specimen mixture proportions, as well as details of specimen preparation and testing. After that, Section 5.3 presents the experimental results of all specimens. Next, a discussion of these results is presented in Section 5.4. Finally, the conclusions of this chapter are presented in Section 5.5.

5.2 DESCRIPTION OF EXPERIMENTAL PROGRAM

5.2.1 Test Matrix

The test matrix for the radiography tests is shown in Table 5.1. As shown in the table, four different groups of cylindrical specimens were tested (CG, B10, B20, and CONC). CG refers to the specimen that was conventional grout, made with only Type I Portland cement and water. B10 and B20 refer to specimens made with 10% and 20% by weigh barium carbonate ($BaCO_3$), respectively. CONC refers to the specimen that was made with Type I Portland cement and water as well as fine and coarse aggregates. This specimen was included to compare the attenuation properties of grout and concrete. Also, the CONC specimen was the same specimen made and tested by Keller and Pessiki (2016), so it is included here for comparison purposes.

5.2.2 Mixture Proportions

Mixture proportions of all cylindrical specimens are shown in Table 5.2. As shown in the table, 3 different grout batches as well as a concrete specimen were tested. All specimens had a nominal diameter of 15 cm and length of 30 cm. Specimen CONC had a water/cement ratio of 0.34. All of the grout specimens had a water/cement ratio of 0.45, which is consistent with previous tests.

5.2.3 Specimen Preparation

All mixing tools and dry ingredients as well as mixing water and water in the water bath were prepared and set in the laboratory one day prior to mixing to ensure that all materials were at the same temperature. On the day of mixing, all ingredients were mixed using a benchtop mixer as follows: the dry ingredients were mixed manually first to make certain they were well blended. Then, the water was added to the mixer. After that, the dry ingredients were added gradually to the mixer within 2 minutes. Materials were mixed for additional 0.5 minutes to assure their uniformity. After that, the mixer was stopped for 1 minute to scrape down into the bowl any material stuck on its side. Finally, materials were mixed again for 2.5 minutes.

Because of the low volume of the benchtop mixer compared to the volume required to make a cylinder, three identical batches were made for each specimen and temporarily placed in a 19-liter bucket. After all three batches were added to the bucket, the grout was blended and cast in a concrete plastic mold in three layers. Because of the absence of aggregate, each layer was consolidated by tapping the outer perimeter of the mold smoothly. A trowel was used to finish specimens surfaces with a sawing motion across the

top of the mold.

Specimens were cured in a lime-saturated water as shown in Figure 5.1. Before radiographic imaging, the specimens were wet cured for about 28 days and after that air dried for about 5 months.

5.2.4 Specimen Testing

All radiography tests were performed at an industrial facility using a 320 keV bipolar COMET MXR-320 X-ray tube (target angle of 20°) inside a 6 m × 6 m vault. The voltage and current of the x-ray tube for all tests were fixed at 320 kiloelectron volts (keV) and 10 milliamperes (mA). The exposure time was varied according to the target optical density (OD) for each particular test. In order to prevent the very low energy photons from reaching the cylinder, a 3.0 mm Be filter was used. The X-ray film used in all imaging was a 30 cm × 25 cm Agfa D4, and the source to film distance (SFD) was 1 m for all tests.

A 90 cm diameter concrete block assembly with a circular opening at its center, was used to enclose the specimens during testing. This enclosure served to shield the specimen and film from stray photons in the testing room. A scheme of the assembly, taken from Pessiki and Keller (2015), is shown in Figure 5.2. In order to place specimens easily, the circular opening was roughly 4 mm larger than the diameter of the specimen. In order to insert and extract the film, a removable wall panel was constructed in the assembly along with an opening has the same size as the film and the removable plywood board on which the film is mounted.

Determination of Exposure Times

In order to determine the time through which specimens will be exposed to the X-rays, Specimen CONC was imaged initially at 320 keV-10.0 mA for 480 seconds. The resulting optical density of Specimen CONC at its center was 1.53. Assuming a linear relationship between exposure time and optical density, the following exposure times were used in this research:

(1) For a target density of 1.00 :

$$\frac{480 \text{ seconds}}{1.53} = \frac{t1}{1.00}$$

$$\therefore t1 = 314 \text{ seconds}$$

Therefore, an exposure time of 320 seconds was determined for a target density of 1.00.

(2) For a target density of 2.00 :

$$\frac{480 \text{ seconds}}{1.53} = \frac{t2}{2.00}$$

$$\therefore t2 = 627 \text{ seconds}$$

Therefore, an exposure time of 640 seconds was determined for a target density of 2.00.

(3) For a target density of 3.00 :

$$\frac{480 \text{ seconds}}{1.53} = \frac{t3}{3.00}$$

$$\therefore t3 = 941 \text{ seconds}$$

Therefore, an exposure time of 900 seconds was determined for a target density of 3.00.

After each film was developed, the optical density of the film at each specific exposure time was measured using a densitometer as shown in Figure 5.3. Results were taken along the diameter of the specimen at 15 mm increments from the center in both vertical and horizontal axes as shown in Figure 5.4.

5.3 EXPERIMENTAL RESULTS

Section 5.3.1 presents the results for the conventional grout. Results for the grouts made with barium carbonate are presented in Sections 5.3.2 and 5.3.3. Results for the concrete specimen are presented in Section 5.3.4.

5.3.1 Specimen CG

Specimen CG was exposed to x-ray radiation for two different durations; 320 and 640 seconds. Because of the high optical density of the film, exposing Specimen CG for 900 seconds made it impossible to distinguish the boundaries of the imaged cylinder on the film. Therefore, results for 900 seconds are not included. Table 5.3 presents the optical density measurements for Specimen CG at increments of 15 mm along the x- and y- axes. Figure 5.5 is a plot of the optical density measurements for Specimen CG for both axes and the two different exposure times. The image identification numbers displayed in the figure are comprised of the exposure time (e.g. 640s) and the axis along which the result is taken (e.g. X)

5.3.2 Specimen B10

Specimen B10 was exposed to x-ray radiation for three different durations; 320, 640, and 900 seconds. Table 5.4 presents the optical density measurements for Specimen B10 at increments of 15 mm along the x- and y- axes. Figure 5.6 is a plot of the optical density measurements for Specimen B10 for both axes and the three different exposure times.

5.3.3 Specimen B20

Specimen B20 was exposed to x-ray radiation for three different durations; 320, 640, and 900 seconds. Table 5.5 presents the optical density measurements for Specimen B20 at increments of 15 mm along the x- and y- axes. Figure 5.7 is a plot of the optical density measurements for Specimen B20 for both axes and the three different exposure times.

5.3.4 Specimen CONC

As it mentioned previously, Specimen CONC was exposed to x-ray radiation for 480 seconds in order to specify the other exposure times. In total, Specimen CONC was exposed to x-ray radiation for four different durations; 320, 480, 640, and 900 seconds. Table 5.6 presents the optical density measurements for Specimen CONC at increments of 15 mm along the x- and y- axes. Figure 5.8 is a plot of the optical density measurements for Specimen CONC for both axes and the four different exposure times.

5.4 DISCUSSION OF RADIOGRAPHY TEST RESULTS

The results obtained from the radiography tests on the four specimens are discussed in this section. A comparison of all optical density measurements is discussed in Section 5.4.1. The relationship between the optical density of a film and the exposure time is presented. The effect of adding barium carbonate on attenuation properties is discussed in Section 5.4.2.

Because results along x- and y-axes are similar, to simplify presentation here, only x-axis results are used here.

5.4.1 Comparing Optical Density Measurements for all Specimens

Table 5.7 presents the optical density measurements for all four specimens along the x-axis for 320, 640, and 900 second exposures. Results obtained from all specimens for 320, 640, and 900 second exposures of radiation are plotted in Figures 5.9, 5.10, and 5.11, respectively.

It is noted that comparing specimens B10, B20, and CONC, the specimen containing conventional grout (Specimen CG) has the highest optical density during both 320 and 640 second exposures, indicating that it is weaker attenuator. In other words, more photons were able to penetrate Specimen CG and reached the film surface of the other specimens (B10, B20, and CONC). On the contrary to Specimens CONC, B10, and B20, exposing Specimen CG to radiation for a duration of 900 seconds would produce a very low contrast image; meaning that a very dark radiographic film would be produced. This high optical density complicates the ability to distinguish defects, such as voids, from the surrounding area.

Furthermore, results illustrate that comparing to specimens CG, B10, and CONC, grouts made with 20% barium carbonate (Specimen B20) has the lower optical density; indicating that Specimen B20 is a strong attenuator since fewer photons were able to penetrate it and reaching the film.

5.4.2 Effect of Barium Carbonate on Photon Attenuation

Table 5.8 presents the optical density measurements for all four specimens taken at the center of each specimen (i.e. the intersection of the x- and y-axes) for the three exposure times. The same results are plotted in Figure 5.12. It is noted that the optical density is proportional to the exposure time. For instance, optical density measurements for Specimen B10 are 0.80, 1.52, and 1.65 at exposure times of 320, 640, and 900 seconds, respectively. Moreover, it can be seen that attenuation is considerably increased using barium carbonate as an addition to the grout.

A comparison between the optical density measurements of grouts made with barium carbonate and Specimen CG is presented in Table 5.9. For example, the following equation illustrates procedure used to specify the relative change (RC) of Specimen B10 compared to Specimen CG for a 320 second exposure:

$$RC, \% = \frac{CG - B10}{CG} * 100$$

$$RC, \% = \frac{2.04 - 0.80}{2.04} * 100$$

$\therefore$ RC of Specimen B10 for 320 second exposure = 61%

Results in Table 5.9 show that the 10% barium carbonate provided 61% decrease in the film response for 320 and 640 seconds of radiation comparing to the conventional grout. On the other hand, the 20% $BaCO_3$ provided 76% and 78% decrease in the film response for 320 and 640 seconds of radiation, respectively, comparing to the conventional grout.

5.5 ADDITIONAL OBSERVATIONS FROM RADIOGRAPHY TESTS

In general, it is to be noted that as we move farther from the cylinder's center, differences in optical density measurements for all specimens are larger. This increasing is affected by the air gap between specimen and the assembly through which higher radiation exposure is approaching.

Note that a void would show up as a darker region because the absence of material would result in greater exposure of the film. In a similar manner, the conventional grout also shows up as a darker image relative to the concrete. The advantage of the PAI is that it may further distinguishes the grout from the void.

Various observations are included from previous tables: (1) Specimen CG is a weaker attenuator than Specimen CONC; (2) both B10 and B20 are stronger attenuators than concrete; and, (3) in respect to attenuation, B20 is better than B10 (as expected).

5.6 CONCLUSIONS FROM THE RADIOGRAPHY TESTS

The following conclusions are drawn from the radiography tests:

1. Adding barium carbonate to grout increased the photon attenuation ability of the grout. This confirms previous results by Keller and Pessiki.
2. As the quantity of barium carbonate increased, the photon attenuation ability of grout also increased. This also confirms previous results by Keller and Pessiki.
3. The conventional grout, made with Type I Portland cement and water, is a weak attenuation material to the extent that when it was exposed for 900 seconds of x-ray radiation, it was impossible to distinguish the boundaries of the imaged cylinder on the film.

Table 5.1 - Test matrix for radiography tests.

Group	Comments
CG	**Type I Portland cement + water**
B10	**Type I Portland cement + 10% barium carbonate + water**
B20	**Type I Portland cement + 20% barium carbonate + Water**
CONC	**Type I Portland cement + aggregate + water**

Table 5.2 - Mixture proportions for radiography tests.

	Percent by Weight						
Group	**Cement**	**Fine aggregate (sand)**	**Coarse aggregate (#57 stone)**	**Coarse aggregate (#8 stone)**	**$BaCO_3$**	**Water**	**Comments**
CG	**55.0**	**0.0**	**0.0**	**0.0**	**0.0**	**45.0**	**Conventional grout**
B10	**64.5**	**0.0**	**0.0**	**0.0**	**6.4**	**29.0**	**10% Barium carbonate**
B20	**60.6**	**0.0**	**0.0**	**0.0**	**12.1**	**27.3**	**20% Barium carbonate**
CONC*	**18.7**	**28.2**	**28.0**	**18.8**	**0.0**	**6.3**	**Concrete**

* Taken from a previous work of (Keller & Pessiki, 2015)

Figure 5.1 - Specimens CG (left), B10 (middle), and B20 (right) during curing.

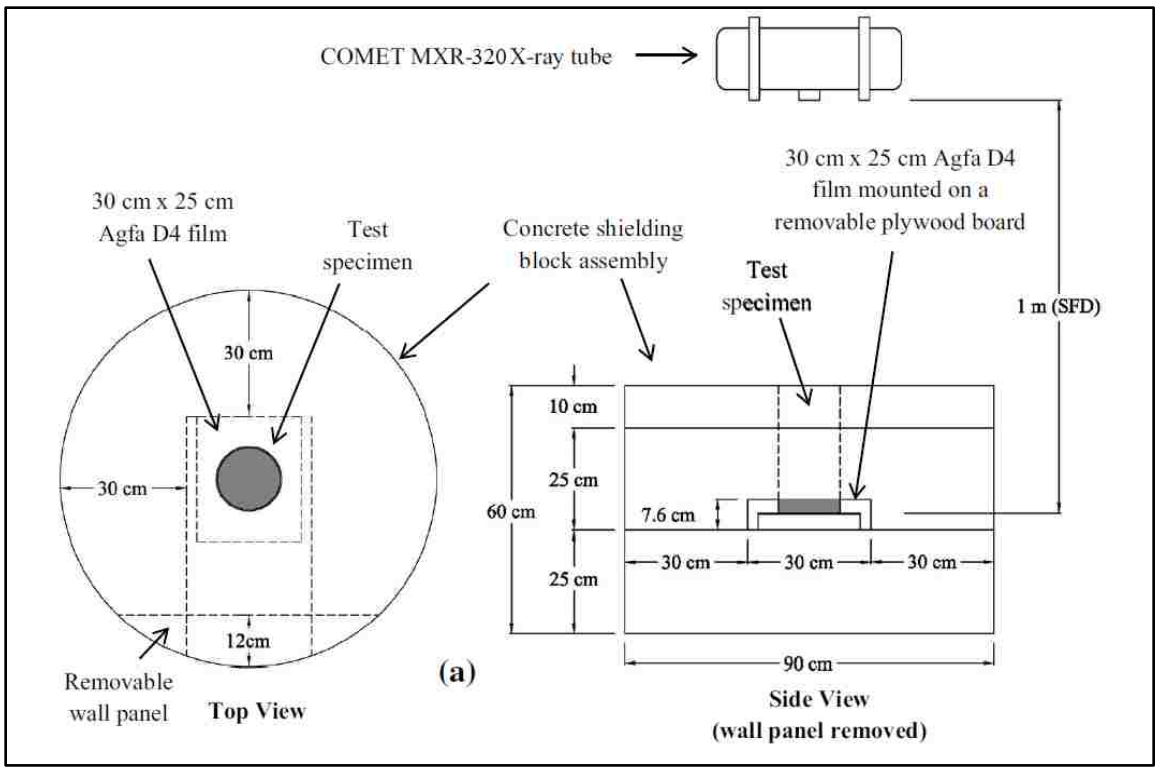

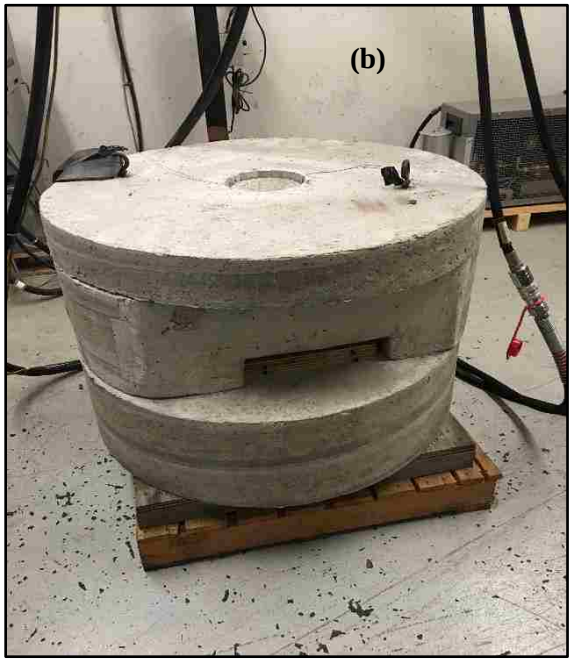

Figure 5.2 - Radiographic imaging: (a) shielding block assembly geometry (Keller & Pessiki, 2015), (b) shielding block assembly before installing the removable wall panel, and (c) final test configuration.

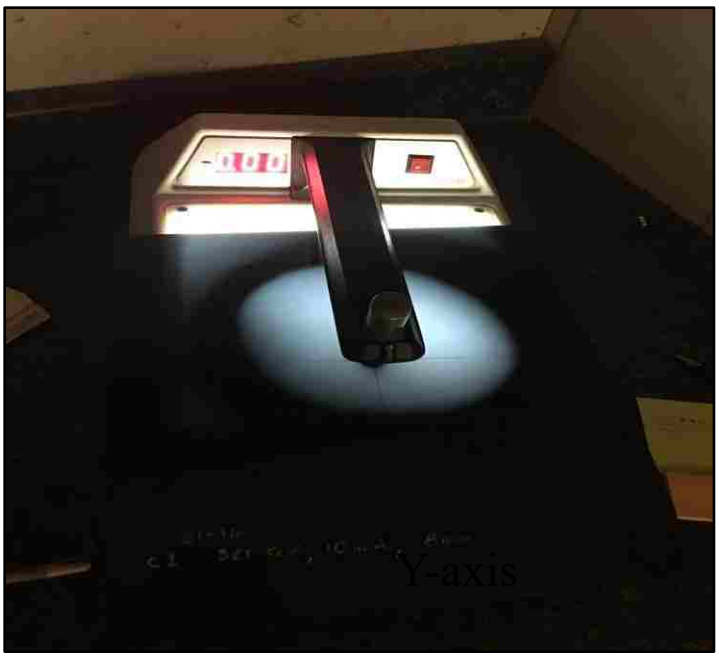

Figure 5.3 - Photograph of the densitometer used to make optical density measurements.

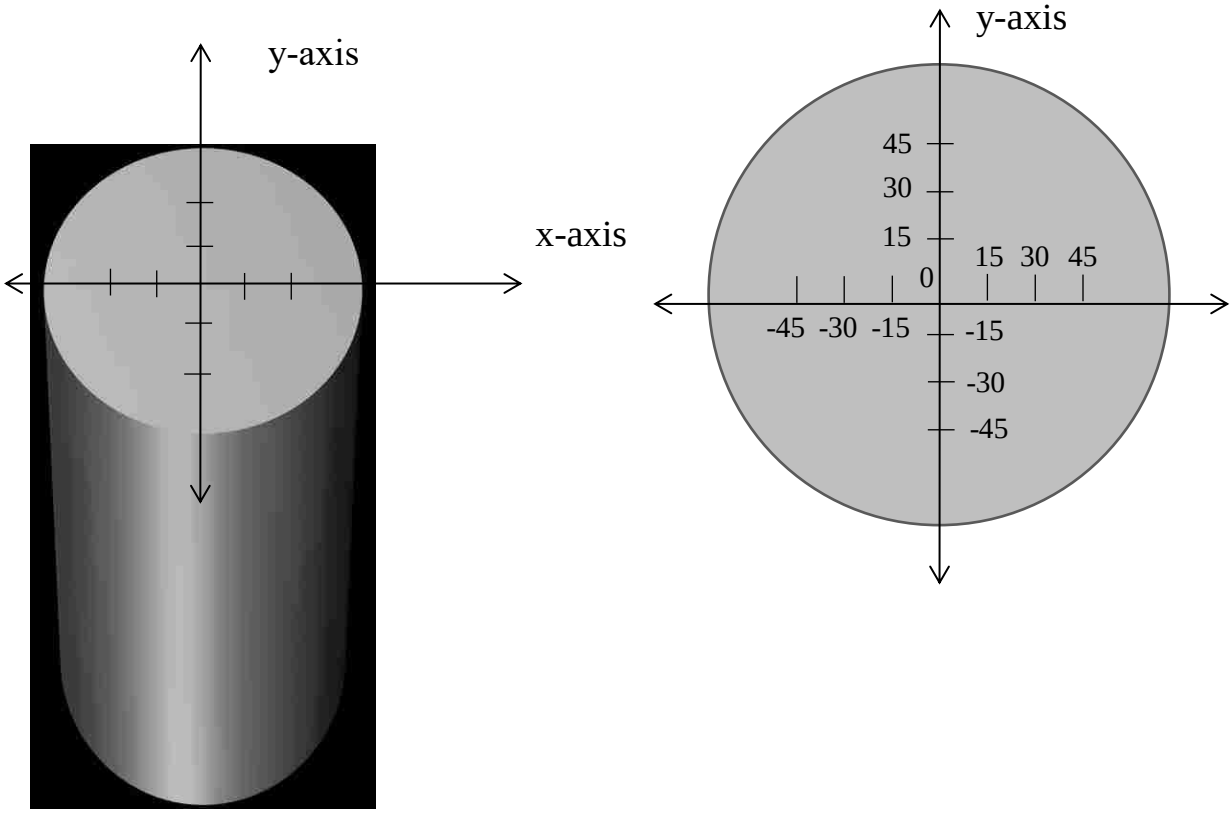

Figure 5.4 - Optical density was measured along the diameter of the cylinders along x- and y-axes.

Table 5.3 - Optical density measurements for Specimen CG.

	Exposure Time (seconds)		Location from Centerline (mm)				
			-30	-15	0	15	30
Optical Density	320	X-axis	2.19	2.10	2.04	2.03	2.04
		Y-axis	2.17	2.10	2.04	2.01	2.00
	640	X-axis	4.28	4.07	3.93	3.87	3.88
		Y-axis	4.47	4.18	3.93	3.75	3.60

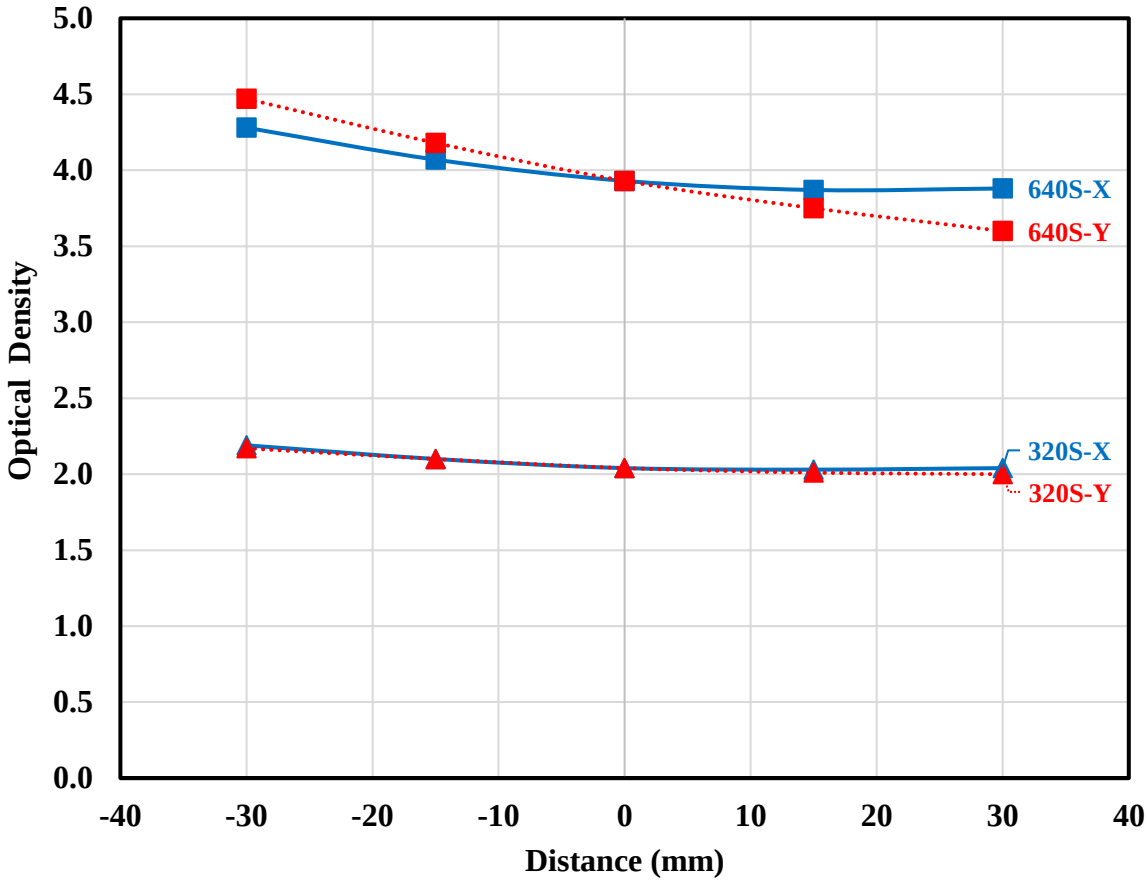

Figure 5.5 - Optical density measurements for Specimen CG along x- and y-axes.

Table 5.4 - Optical density measurements for Specimen B10.

	Exposure Time (seconds)		Location from Centerline (mm)				
			-30	-15	0	15	30
Optical Density	320	X-axis	1.12	0.92	0.80	0.75	0.74
		Y-axis	0.87	0.82	0.80	0.81	0.83
	640	X-axis	2.38	1.83	1.52	1.35	1.28
		Y-axis	1.64	1.54	1.52	1.55	1.65
	900	X-axis	1.84	1.70	1.65	1.68	1.80
		Y-axis	1.70	1.63	1.65	1.73	1.86

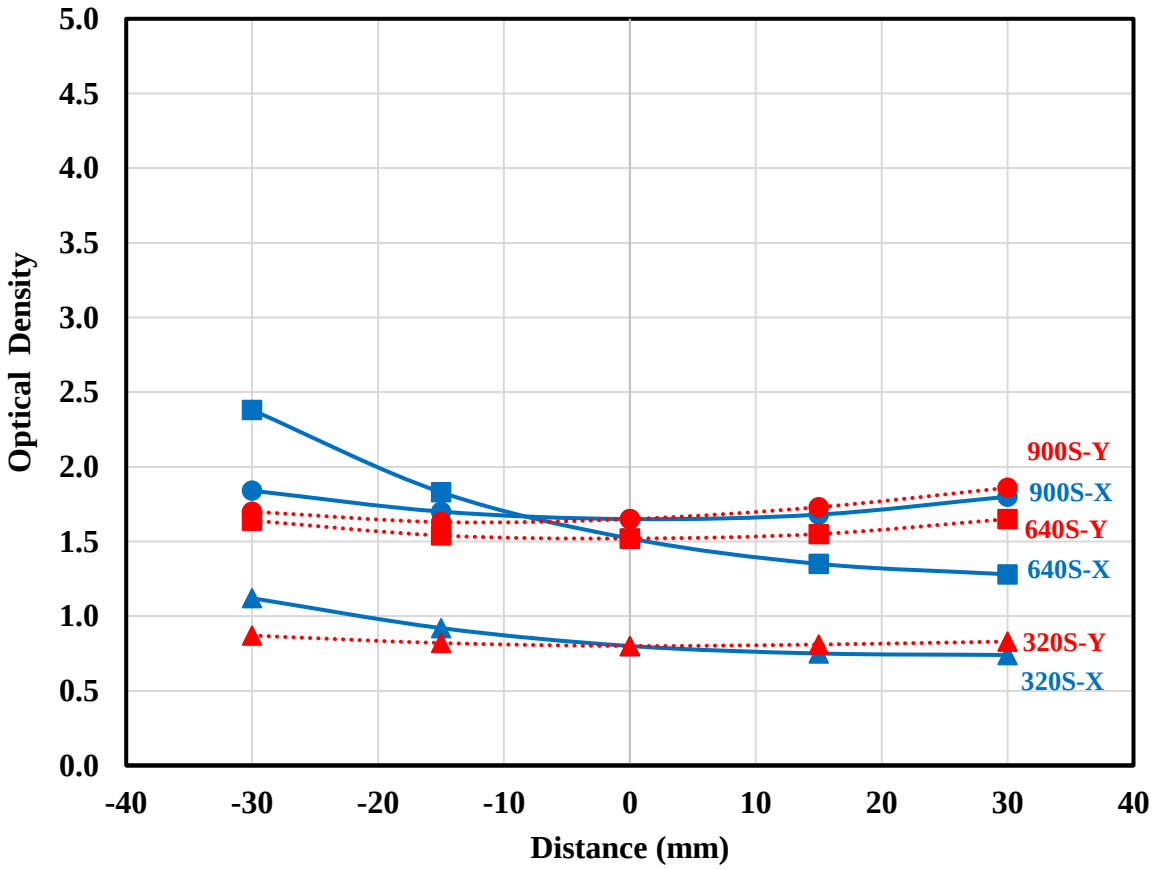

Figure 5.6 - Optical density measurements for Specimen B10 along x- and y-axes.

Table 5.5 - Optical density measurements for Specimen B20.

	Exposure Time (seconds)		Location from Centerline (mm)				
			-30	-15	0	15	30
Optical Density	320	X-axis	0.66	0.55	0.49	0.47	0.48
		Y-axis	0.61	0.54	0.49	0.48	0.48
	640	X-axis	1.21	0.97	0.85	0.80	0.81
		Y-axis	1.10	0.93	0.85	0.80	0.80
	900	X-axis	1.27	1.12	1.07	1.06	1.12
		Y-axis	1.55	1.24	1.07	0.98	0.96

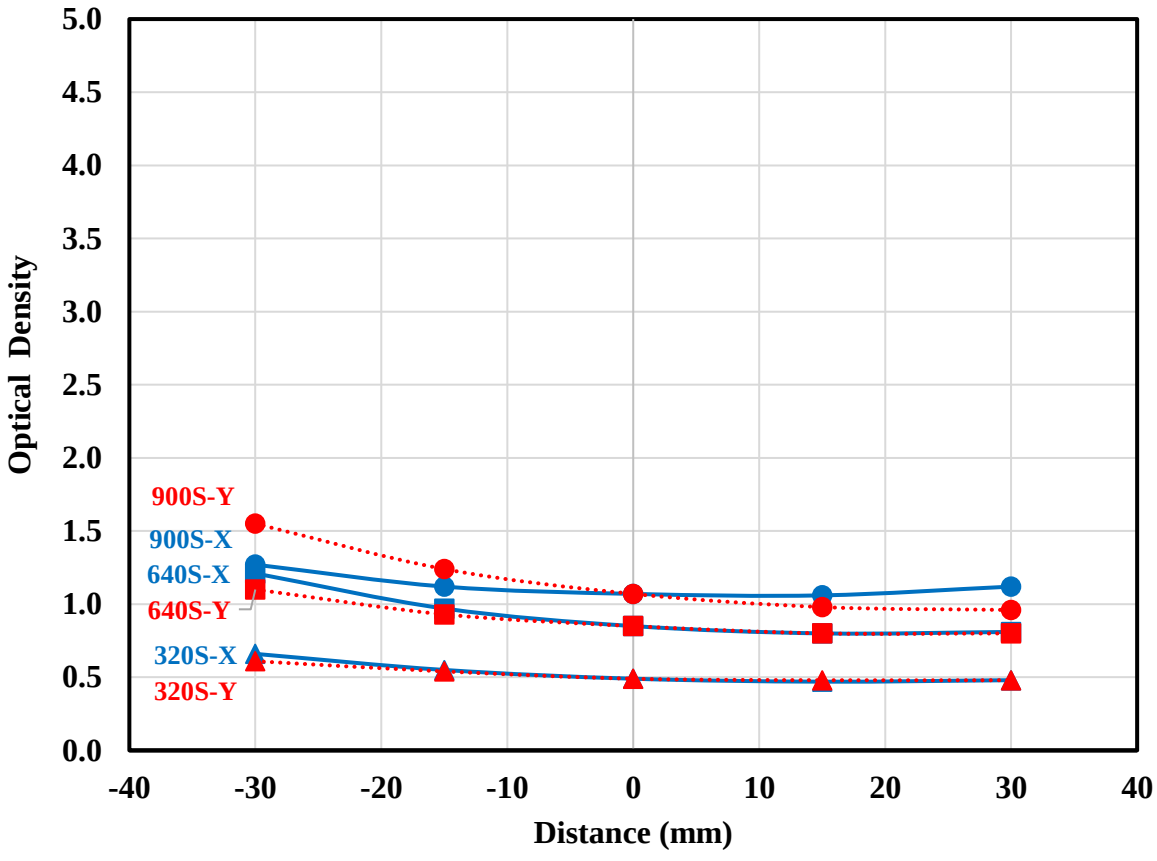

Figure 5.7 - Optical density measurements for Specimen B20 along x- and y-axes.

Table 5.6 - Optical density measurements for Specimen CONC.

	Exposure Time (seconds)		Location from Centerline (mm)				
			-30	-15	0	15	30
Optical Density	320	X-axis	1.33	1.18	1.11	1.09	1.12
		Y-axis	1.07	1.06	1.11	1.18	1.28
	480	X-axis	1.78	1.62	1.53	1.54	1.58
		Y-axis	1.71	1.60	1.53	1.55	1.56
	640	X-axis	2.24	2.08	2.02	2.04	2.13
		Y-axis	2.00	1.99	2.02	2.12	2.30
	900	X-axis	4.75	3.79	3.23	2.83	2.58
		Y-axis	4.02	3.56	3.23	3.03	2.90

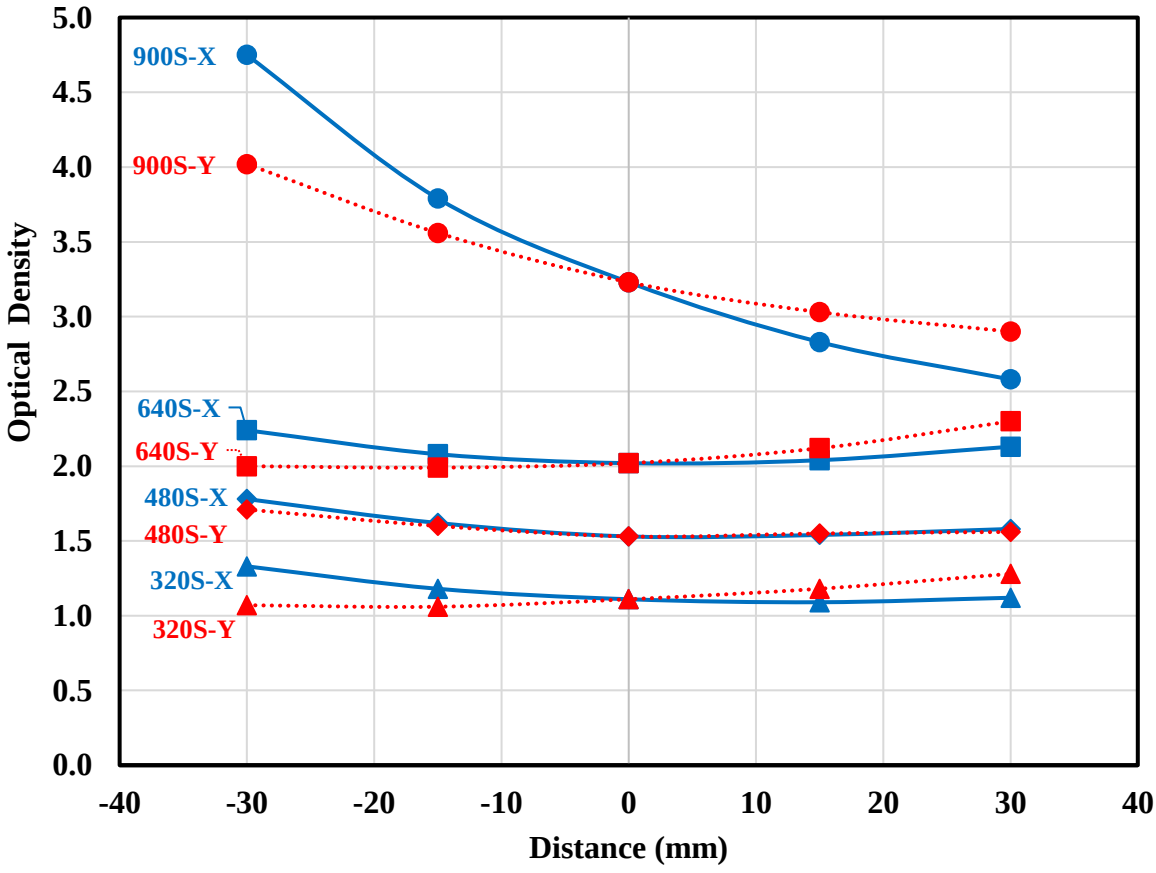

Figure 5.8 - Optical density measurements for Specimen CONC along x- and y-axes.

Table 5.7 - Optical density measurements for all specimens along the x-axis.

	Specimen ID	Exposure Time (seconds)	Location from Centerline (mm)				
			-30	-15	0	15	30
Optical Density	CG	320	2.19	2.10	2.04	2.03	2.04
		640	4.28	4.07	3.93	3.87	3.88
		900	-	-	-	-	-
	B10	320	1.12	0.92	0.80	0.75	0.74
		640	2.38	1.83	1.52	1.35	1.28
		900	1.84	1.70	1.65	1.68	1.80
	B20	320	0.66	0.55	0.49	0.47	0.48
		640	1.21	0.97	0.85	0.80	0.81
		900	1.27	1.12	1.07	1.06	1.12
	CONC	320	1.33	1.18	1.11	1.09	1.12
		640	2.24	2.08	2.02	2.04	2.13
		900	4.75	3.79	3.23	2.83	2.58

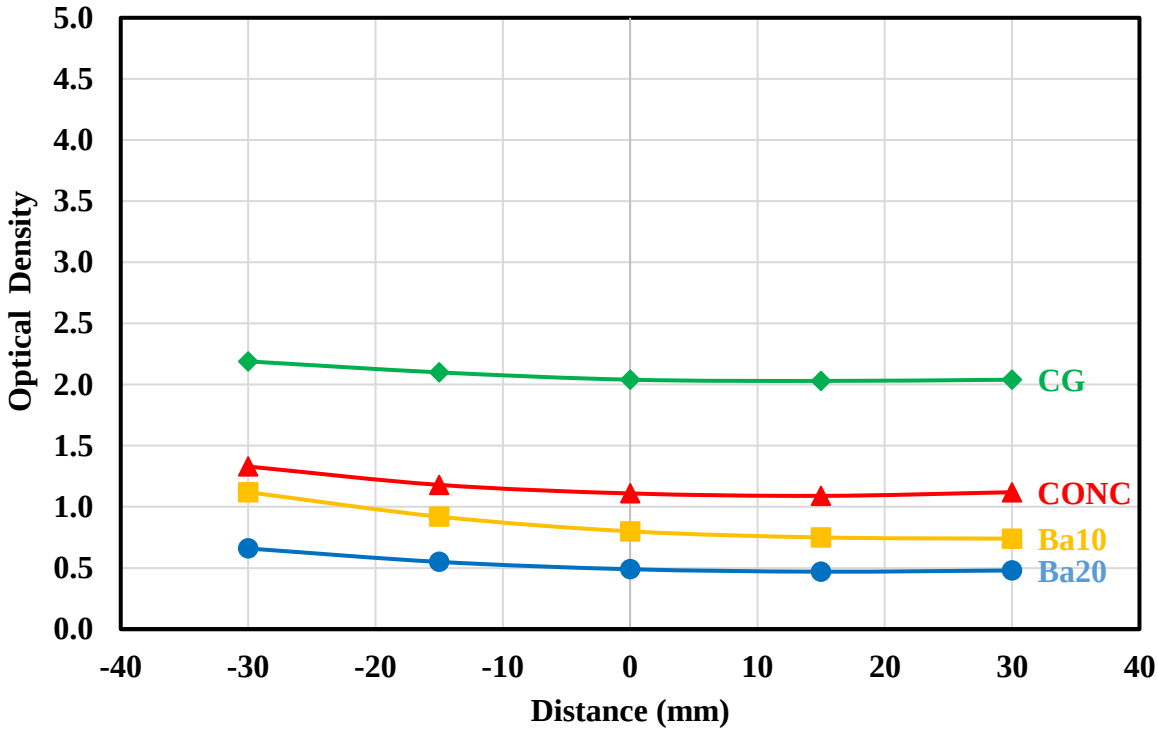

Figure 5.9 - Optical density measurements for all specimens along the x-axis for a 320 second exposure.

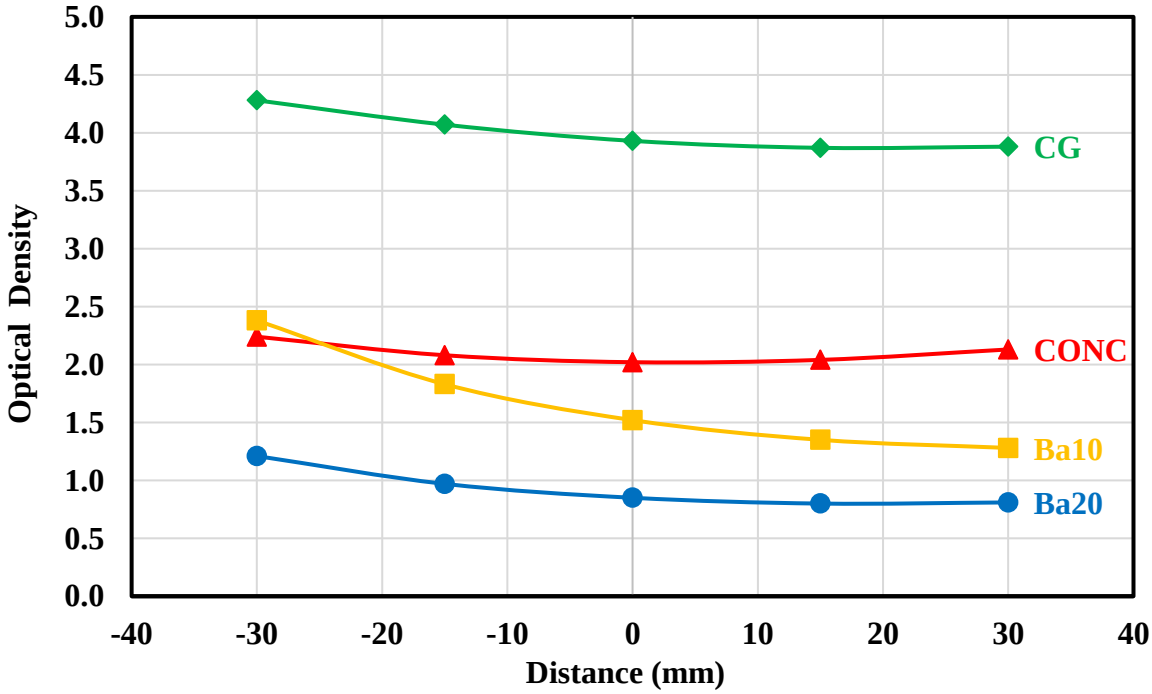

Figure 5.10 - Optical density measurements for all specimens along the x-axis for a 640 second exposure.

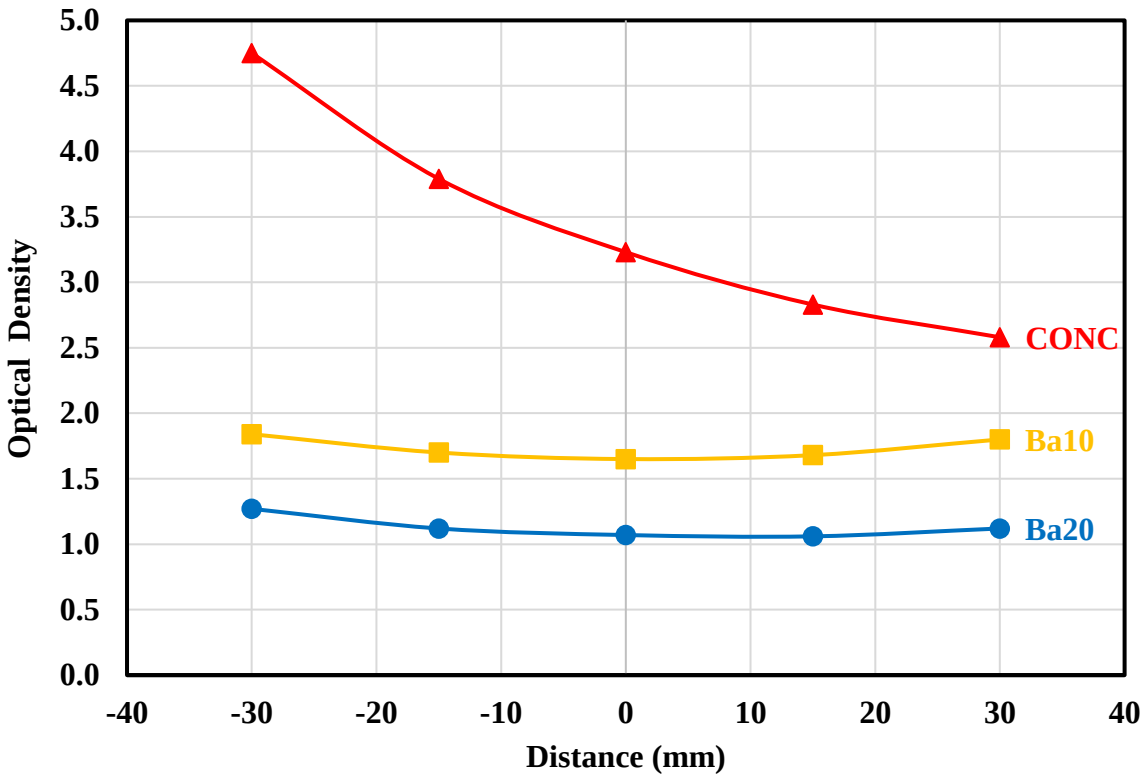

Figure 5.11 - Optical density measurements for all specimens along the x-axis for a 900 second exposure.

Table 5.8 - Optical density measurements for all specimens at the intersection of x- and y-axes.

	ID	Exposure Time (seconds)		
		320	640	900
Optical Density	CG	2.04	3.93	-
	B10	0.80	1.52	1.65
	B20	0.49	0.85	1.07
	CONC	1.11	2.02	3.23

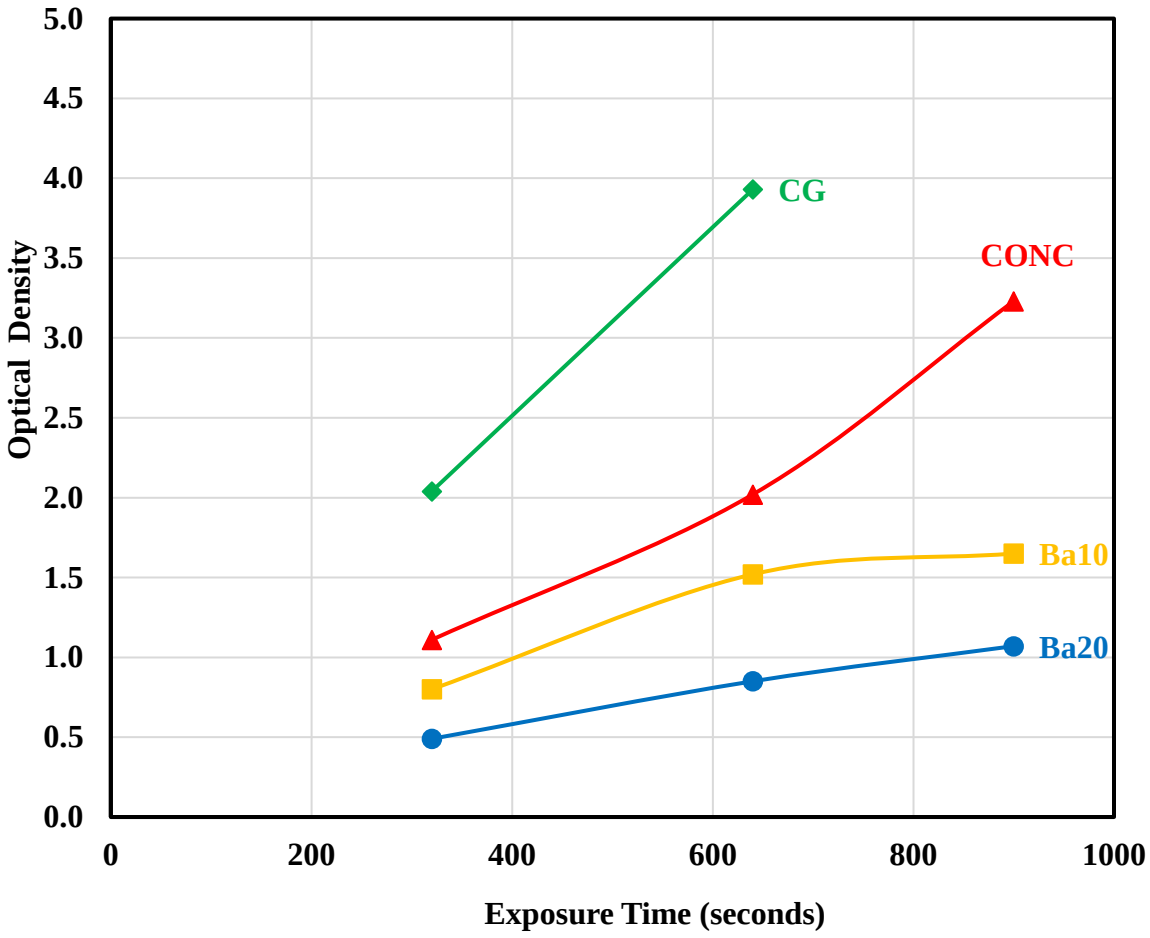

Figure 5.12 - Optical density measurements for all specimens at the intersection of x- and y-axes versus exposure time.

Table 5.9 - Comparison of optical density measurements for Specimen CG to other specimens at the intersection of x- and y-axes.

Exposure Time (seconds)	Optical Density Measurement			Relative Change in Optical Density Measurements with Reference to Specimen CG (%)	
	CG	B10	B20	B10	B20
320	2.04	0.80	0.49	61	76
640	3.93	1.52	0.85	61	78

CHAPTER 6

SUMMARY, CONCLUSIONS, AND FUTURE WORK

This chapter presents a brief summary of the research, a concise review of the conclusions, and outlines future research needs related to the research.

6.1 SUMMARY

This research explores the effect of adding photon attenuating inclusions, specifically barium carbonate and iron oxide as well as Ottawa Sand within cementitious grout used in PT structures. Three various properties; compression strength, bleeding characteristics, and photon attenuation characteristics, were the investigated properties. Compression strength tests were explained in Chapter 3 while bleed tests and radiography tests were presented in Chapter 4 and Chapter 5, respectively.

For compression strength tests and bleed tests, the objective was to investigate whether grout would meet the requirements of PTI M55. The objective of the radiography test was to study the effect of barium carbonate on the photon attenuation ability of the grout.

6.2 CONCLUSIONS

The following conclusions are drawn from the grout compression tests:

1. Adding barium carbonate to the grout did not have an adverse effect on the compression strength of the grout at 28 days as well as at early ages (3 and 7 days).

2. Results of grout having barium carbonate (10% and 20% of cement weight) satisfied the compression strength requirements of PTI M55 at ages 7 and 28 days.
3. For the two quantities of barium carbonate considered, there was no clear relationship between quantity of barium carbonate and compressive strength of the grout.
4. Adding iron oxide to the grout did not have an adverse effect on the compression strength of the grout at 28 days as well as at early ages (3 and 7 days).
5. Results of grout having iron oxide (10% and 20% of cement weight) satisfied the compression strength requirements of PTI M55 at ages 7 and 28 days.
6. For the two quantities of iron oxide considered, there was no clear relationship between quantity of iron oxide and compressive strength of the grout.
7. Results of grout having Ottawa Sand satisfied the compression strength requirements of PTI M55 at ages 7 and 28 days. Moreover, the highest result was achieved by Specimen OS at an age of 28 days.

The following conclusions are drawn from the grout bleed tests:

1. Adding barium carbonate to grout increased its ability to resist bleeding.
2. Grouts made with barium carbonate experienced much less bleed water than the conventional grout although it might not meet the requirement of PTI M55, which is 0.0% at three hours.
3. Not achieving the PTI M55 requirement regarding bleed water might be attributed to the high water/cement ratio used in this research.

The following conclusions are drawn from the grout radiography tests:

1. Conventional grout, made with Type I Portland cement and water, is a weak attenuation material.
2. Adding barium carbonate to grout significantly increased its ability to attenuate the x-ray radiation.
3. As the quantity of barium carbonate increased, the ability of grout to attenuate the x-ray radiation increased.

Finally, it was noted in all three tests that despite the high water/cement ratio, adding barium carbonate to grout had an adverse effect on its workability; in other words, grouts made with barium carbonate were stiffer than conventional grout.

6.3 FUTURE WORK

Future research needs related to this project include the following:

1. Performing the other seven tests required by PTI M55 on grouts made with barium carbonate.
2. Performing strand bond tests on grouts made with barium carbonate.
3. Evaluating the use of admixtures to increase the flow characteristics of grouts made with barium carbonate, and exploring increases in the quantity of barium carbonate in order to achieve even higher photon attenuation.
4. Performing radiography tests on large-scale post-tensioned assemblages made with both conventional grouts and PAI grouts.

REFERENCES

ACI. (2001). "ACI 222R-01 – Corrosion of Prestressing Steels," ACI Committee 222, American Concrete Institute, Farmington Hills, MI.

Assaad, J. J., Daou, Y., & Harb, J. (2015). Influence of thixotropy on performance of grouts placed using vacuum injection techniques. *ACI Materials Journal*, *112*(2), 189–198.

Azizinamini, A., & Gull, J. (2012). Improved Inspection Techniques for Steel Prestressing/Post-tensioning Strand. *FDOT Contract BDK80*, 977–13.

Brown, K., & St Leger, J. (2003, September). Use of the megascan imaging process in inspection systems for post-tensioned bridges and other major structures. *Non-Destructive Testing in Civil Engineering. International Symposium*, (NDT-CE 2003).

Cercone, C., Naito, C., Corven, J., Pessiki, S., Keller, W., & Pakzad., S. (2015). Designing and Detailing Post Tensioned Bridges to Accommodate Non-Destructive Evaluation. ATLSS Report 14-01. Center for Advanced Technology for Large Structural Systems, Lehigh University, Bethlehem.

Corven, J., & Moreton, A. (2013). Post-tensioning Tendon Installation and Grouting Manual.

FDOT. (2002). New Directions for Florida Post-Tensioned Bridges. *Florida Department of Transportation. Post-Tensioning in Florida Bridges. By Corven Engineering, Inc., Tallahassee, Florida.*

Ganz, H. R., & Vildaer, S. (2002). Grouting of post-tensioning tendons. *VSL Report Series*, *5*.

Keller, W. J., & Pessiki, S. (2015). Experimental Validation of a Numerical Model for Simulating Radiographic Imaging of Portland Cement-Based Materials. *Journal of Nondestructive Evaluation*, *34*(3), 1–13.

Keller, W. J., & Pessiki, S. (2016). Enhancing Radiographic Imaging of Cementitious Materials in Composite Structures with Photon Attenuating Inclusions. *Submitted to Research in Nondestuctive Evaluation, December 2016*.

Limaye, H. S., & Kakade, A. M. (2008). Challenges in Nondestructive Testing of Post-Tensioned Bridges. In *2008 Concrete Bridge Conference*.

Mariscotti, M. A. J., Jalinoos, F., Frigerio, T., Ruffolo, M., & Thieberger, P. (2008). Gamma-ray imaging for void and corrosion assessment in PT girders. *NDE/NDT for Highways and Bridges-Structural Materials Technology (SMT)*.

Newman, J., & Choo, B. S. (Eds.). (2003). *Advanced concrete technology 3: processes*. Butterworth-Heinemann.

Pimentel, M., Figueiras, J., Mariscotti, M., Thieberger, P., Ruffolo, L. M., & Frigerio, T. (2010). Gamma-ray inspection of post tensioning cables in a concrete bridge. *Structural Faults & Repair 2010*.

Priyada, P., Ramar, R., & Shivaramu. (2013). Application of gamma ray scattering technique for non-destructive evaluation of voids in concrete. *Applied Radiation and Isotopes*, *74*, 13–22.

PTI M55 (2012). *Specification for Grouting of Post-Tensioned Structures*, Post-Tensioning Institute, Farmington Hills, MI.

PTI (2015). Selection of Filler Materials for Multistrand PT Tendons. *Technical Advisory Board. PTI Technical Notes*, (19), 5.

Saravanan, K., Srinivasan, S., Kapali, V., Nayak, N. U., Sureshbapu, R. H., Madhavamayandi, A., Kalyanasundaram, R. M., Rengaswamy, N. S., & Balakrishnan, K. (1996). Non-Destructive Examination of Corroded Concrete Structuers using Radiography. *Bulletin of Electrochemistry*, *12*(1–2), 8–10.

Schokker, A. J., Breen, J. E., & Kreger, M. E. (2001). Grouts for bonded post-tensioning in corrosive environments. *Materials Journal*, *98*(4), 296–305.

Schokker, A. J., Hamilton, H. R., & Schupack, M. (2002). Estimating post-tensioning grout bleed resistance using a pressure-filter test. *PCI Journal*, *47*(2), 32–39.

Schupack, M. (2004). PT grout: Bleed water voids. *Concrete International*, *26*(8), 69–77.

Theryo, T. S., Hartt, W. H., & Paczkowsk, P. (2013). *Guidelines for Sampling, Assessing, and Restoring Defective Grout in Prestressed Concrete Bridge Post-Tensioning Ducts*. (No. FHWA-HRT-13-028).

Trejo, D., Hueste, M. B., Gardoni, P., Pillai, R., Reinschmidt, K., Im, S. B., Kataria, S., Hurlebaus, S., Gamble, M., & Ngo, T. (2009). *Effect of voids in grouted post-tensioned concrete bridge construction*. *Texas Department of Transportation (TxDOT). Austin, TX*.

Uesaka, M., Jin, M., Wu, W., & Dobashi, K. (2013). Commissioning of portable 950 keV/3.95 MeV X-band linac X-ray sources for on-site transmission testing. *E-Journal of Advanced Maintenance*, *5*(2), 93–100.

Washer, G. A. (2003). Improving bridge inspections. *Public Roads*, *67*(3).

VITA

Abdulrahman Abdulmohsen Alfurayh was born in Buraidah, Saudi Arabia on January 24, 1989. He is the son of Abdulmohden and Hissah. He has six younger siblings. He earned his Bachelor degree in Civil Engineering in February 2012 from Qassim University. After graduation, he worked in Qassim University as a teaching assistant in 2012 and was sent to pursue his graduate study in the United States in 2014. After studying English in the University of Delaware for almost one year, he was accepted as a graduate student at Lehigh University in 2015 in the major of structural engineering. He is expected to be awarded his master degree in September 2017.